FINAL REPORT

Covering the Period
April 26, 1966 -- January 26, 1967

STUDY OF
RADIATIVE ASPECTS OF LUNAR MATERIALS

Contract No. NAS8-20385
Req. No. 1-6-28-00057

Donald G. Burkhard
Neil Ashby

Prepared by

P.E.C. RESEARCH ASSOCIATES, INC.
(Physics, Engineering & Chemistry)
1001 Mapleton Avenue
Boulder, Colorado 80302
(442-6015 -- area 303)

Prepared for

GEORGE C. MARSHALL SPACE FLIGHT CENTER
Huntsville, Alabama

N68 - 15550

FACILITY FORM 602

(ACCESSION NUMBER)   (THRU)

121
(PAGES)   (CODE)

CR-121484
(NASA CR OR TMX OR AD NUMBER)   30
                                     (CATEGORY)

CR-73883

TABLE OF CONTENTS

CHAPTER I

Introduction

This report is divided into three main chapters, each with its own references and appendices, with each chapter paged independently of the others. In the following two chapters we discuss the photometric aspects of lunar materials; in the third chapter the infrared aspects are discussed. Fine details of the wavelength dependence of lunar radiation are not considered in this report; rather the two principal wavelength regions of visible and infrared radiation are considered separately.

In Chapter II, we discuss an improved photometric function which appears to represent observations of radiance of the lunar surface by photometric means, as a function of angle of incidence, angle of observation, and phase angle to within rather small limits of error. Calculations of the root mean square deviation of the mathematical expression presented here from the observed radiances, generally vary from 4% to 11%. This function seems to give a satisfactory representation of the radiance of the lunar surface. In this function are two adjustable parameters--the normal albedo and a parameter g, called the compaction parameter, which represents roughly the degree of porosity of the lunar surface. Values of this compaction parameter vary from about .20 to .95 for various types of surface features.

In the appendices to Chapter II are given tables from which may be obtained the total energy reflected per cm^2 per min into all angles, from a surface feature of known normal albedo and compaction parameter, at any given angle of illumination from the sun. Because of the complicated nature of the dependence of the photometric function on angle, and because there are so many angles upon which it depends, we have not computed tables of the photometric function itself except for certain selected surface features.

In Chapter 3 are placed all derivations of the photometric functions considered for numerical calculations, based on a model of the rough lunar surface.

In Chapter 4 we present a mathematical expression which represents to the best of our ability the directional character-istics of the infrared radiation from the lunar surface. A rigorous derivation of this function is not given; however, we present a very simple model from which the main features of this mathematical expression follow. A number of comparisons with observational data--particularly that of Saari and Shorthill--are given. Generally speaking the error in energy units of these results is of the order of 5%; in terms of temperature the error is about a quarter of this.

NUMERICAL CALCULATIONS OF PHOTOMETRIC FUNCTION

B. W. Hapke[1] has given a derivation of a photometric
function for the lunar surface which appears to agree extremely
well with observations.   One may wonder then what possible
improvements could be made in this function.   We will point
out what appears to be a serious deficiency in Hapke's theoreti-
cal retrodirective function and hence in his photometric function.

First we note that the energy reflected per unit time (in
sec) per unit solid angle from a unit area (in cm^2) of the
lunar surface is written according to Hapke in the form

$$I^{(re)}(i,t,\alpha) = \frac{S_o}{\pi} \rho(i,\epsilon,\alpha)\cos\epsilon = B(i,\epsilon,\alpha)\cos\epsilon$$

$$(1)$$

where the factor $\cos\epsilon$ arises purely from the geometry of the
outgoing ray, S_o is the solar constant and ρ is the radiance
factor.   The brightness or radiance $B(i,\epsilon,\alpha)$ is given in terms
of the photometric function $\varphi(i,\epsilon,\alpha)$ by

$$B(i,\epsilon,\alpha) = \frac{S_o}{\pi}a\ \varphi(i,\epsilon,\alpha) \qquad (2)$$

where a is the normal albedo.   The radiance factor ρ is defined
by

$$\rho(i,\epsilon,\alpha) = a\varphi(i,\epsilon,\alpha) \quad . \qquad (3)$$

According to Hapke's results the photometric function may be written as the product of three terms:

$$\varphi(i,\epsilon,\alpha) = \frac{\cos i}{\cos i + \cos \epsilon} \cdot \sum(\alpha)B(\alpha,g). \qquad (4)$$

The factor $\cos i/(\cos i + \cos \epsilon)$ is just the well-known Lommel-Seeliger law, $\sum(\alpha)$ is the scattering law of an individual object, and $B(\alpha,g)$ is the retrodirective function.

A complete discussion of the derivation of the above expressions is given in Chapter 3; in this chapter we wish only to discuss the results of numerical calculations performed using Hapke's retrodirective function, which is given by

$$B(\alpha,g) = \begin{cases} 2 - \dfrac{\tan\alpha}{2g}(1-e^{-g/\tan\alpha})(3-e^{-g/\tan\alpha}) &, \alpha < \pi/2 \\ 1 &, \alpha > \pi/2 \end{cases}$$

$$(5)$$

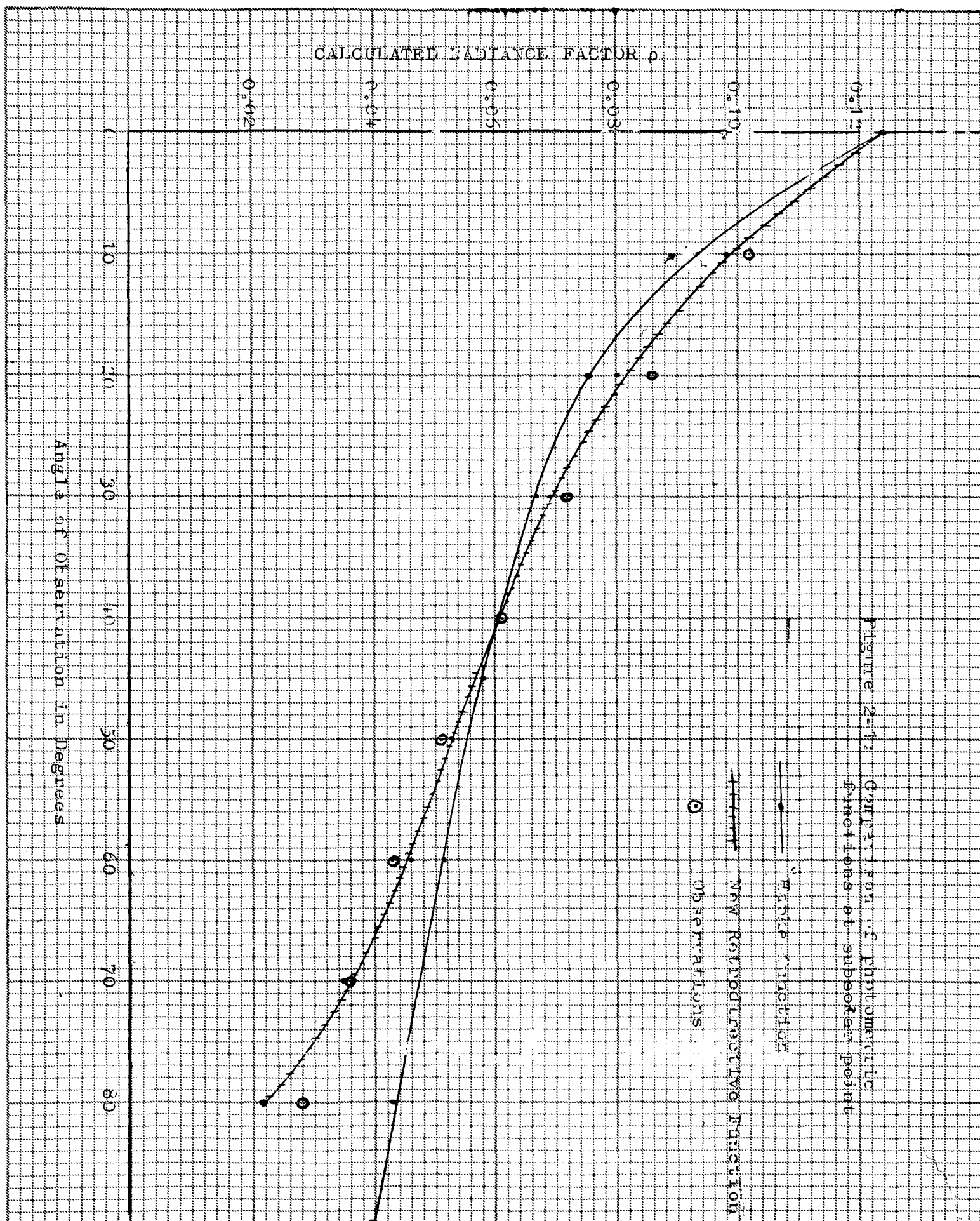Also, the scattering law $\sum(\alpha)$ is given by

$$\sum(\alpha) = \frac{1}{\pi}\{(\pi-\alpha)\cos\alpha + \sin\alpha\} \quad . \qquad (6)$$

Now in comparing the observed radiances with the above photometric function, Hapke used the data of Fedoretz[2] for selected lunar features. This means that the angle of

observation ϵ is fixed, (since the moon does not rotate while the angle of incidence i varies) for a particular surface feature. Quite good fits to the observational data can be obtained. However by comparing different curves, for different surface features-- and hence for different angles of observation ϵ, one notices a systematic dependence of the compaction parameter on angle of observation. For Mare Nectaris, Mare Serenitatis, Ptolmaeus, and Pitatus which are located at angles ϵ less 35°, Hapke gives the compaction parameter g = 0.6. For Mare Imbrium and Tycho, which are located at angles of observation greater than 35°, the compaction parameter is 0.4.

This apparent dependence of compaction parameter on angle of observation is made even more evident whem comparing Hapke's photometric function to the data of Orlova[3] for terrae or maria, particularly if one chooses a fixed angle of <u>incidence.</u> For example in Figure 2-1 is plotted the observed radiance factors for terrae at the subsolar point. A Hapke photometric function which best fits the data on terrae corresponds to a compaction parameter of 0.51 and is also plotted on the same figure. It is seen that at small angles of incidence the Hapke function gives too little radiance while at larger angles of incidence it gives considerably too much radiance. These features made it difficult for us to obtain consistently good fits to radiance data with a Hapke photometric function.

Consequently we re-examined the model on which the derivation of Hapke was based. This duscussion is given in detail in Chapter III. By various modifications of the model, a number of other photometric functions were derived. Numerical

Figure 2-1: Graphs for the photometric functions et subsolar point

CALCULATED RADIANCE FACTOR ρ

Angle of Observation in Degrees

⊙ New Retrodirective Function

—•— Hapke Function

⊙ Observations

calculations were performed with two of these new photometric functions during the course of this work. In the first of these, the first part of Equation (5) is replaced by:

$$B(\alpha, g) = 2.0 - \frac{2\tan\alpha}{g} + \frac{4\sin\alpha}{g(1+2\cos\alpha)^2} + \frac{2\tan\alpha}{g}e^{-g/\tan\alpha}$$

$$+ \left[\frac{-2}{1+2\cos\alpha} + \frac{-4\sin\alpha}{g(1+2\cos\alpha)^2}\right] e^{-g(1+\frac{1}{2\cos\alpha})/\tan\alpha}$$

$$+ \frac{2}{1+\cos\alpha}e^{-\{g/2\sin\alpha + g(1+1/\cos\alpha)/\tan\alpha\}}, \quad \alpha < \pi/2 \quad (7)$$

$$B(\alpha, g) = 1, \quad \alpha > \pi/2 \; .$$

The second of these, which we shall refer to as the "new" retrodirective function, is given by:

$$B = B(i, \epsilon, \alpha, g) = \frac{2}{s}\left[2.0 - \frac{\tan\alpha}{2g}(1-e^{-gs/2\tan\alpha})(3-e^{-gs/2\tan\alpha})\right.$$

$$\left. + (\frac{s}{2}-1)e^{-gs/2\tan\alpha}(2-e^{-gs/2\tan\alpha})\right], \quad \alpha < \pi/2$$

$$(8)$$

$$= \frac{2}{s}, \quad \alpha > \pi/2$$

where $s(i, \epsilon)$ is given by:

$$s(i, \epsilon) = \frac{1}{2}(\cos i + \cos\epsilon)\left(\frac{1}{\cos i} + \frac{1}{\cos\epsilon}\right) \; . \quad (9)$$

We note that if s in Equation (8) is placed equal to 2, the Hapke photometric function is obtained. In the latter form, the "new" retrodirective function has a more complicated dependence on both angle of incidence and angle of reflection than does the retrodirective function of Hapke.

The radiance calculated using the new retrodirective function, Equation (8) is also plotted in Figure 2-1. It is seen that considerably better agreement with the data is obtained, except for ϵ near $90°$.

Energy Reflected from Lunar Terrae and Maria

We used a Hapke photometric function (Equation 5), the function given by Equation (7), and the "new" function given by Equation (8), in comparisons between calculations and observation for lunar terrae and maria. For data we used the tables of Orlova[3] for terrae and maria along the lunar equator. In Table I is given the results for rms error and compaction parameter for these features.

TABLE I

Comparison of Retrodirective Functions with Observation, along
Lunar Equator, for terrae.

Radiance Calculated Using	Compaction Parameter, g	r.m.s. deviation between theory & observation, in cal/cm²min sterad	Type of Formation
Equation 5 (Hapke function)	0.51	.0061	Terrae
Equation 7	0.61	.0054	Terrae
Equation 8 ("new" retro-directive function	0.623	.0034	Terrae

The "new" retrodirective function gives by far the best fit.
Because of this success, and similar successes with maria and
other lunar formations, we used the new retrodirective function,
Equation (8), in all the following calculations.

We found that for maria, the best fit for g was g = 0.43
with a rms error of .0027 cal/cm²min sterad.

In Appendix I are reproduced tables of Orlava for lunar
terrae and maria, together with tables calculated for these
features using the above-mentioned compaction parameters.
We assumed that the maria have an average normal albedo of
0.081, and that the terrae have an average normal albedo of
0.124. In well over a third of the entries in the tables,

the agreement between calculation and observation is •.001 or better.

The resulting expressions for the energy reflected from maria and terrae have been integrated over all angles to obtain the total energy reflected into all angles per cm^2 per min as a function of angle of incidence. The results are given in Table A-5, in the Appendix to Chapter 2.

As the most abundant lunar formations are maria and terrae, the average for the entire moon of the reflected energy lies somewhere between the entries in the two columns in Table A-5. Earlier it had been shown[4] that the average energy reflected from the subsolar point is 0.106 ± .010 cal/cm^2min.

Compaction Parameters for other lunar formations

In the comparison of calculated photometric brightness with observations, one difficulty had previously been that at large angles of incidence, the calculated brightness has been too small. The major portion of this difficulty may be eliminated as follows. The bulk of the experimental data comes from Fedoretz,[2] who used a brightness scale for his radiance measurements which ranged from 0 to 5. In converting this data to radiance factors, van Diggelen compared the data of Fedoretz with observations made by himself[5] to obtain a scale of conversion from Fedoretz's brightness B, to radiance factor ρ. The result was that van Diggelen used the conversion

$$\rho = .03334B + .005 . \qquad (10)$$

(See reference 5, Figure 20). This means that if Fedoretz's observed brightness is zero, van Diggelen's converted value would be .005; this is hardly reasonable. It appears that in converting Fedoretz's data for his own use, van Diggelen thus introduced a systematic error which is particularly significant for conditions of low brightness. Such a systematic error might possibly be due to fogging of the plates used by van Diggelen, but this is speculation.

We have therefore found it necessary to convert Fedoretz's measurements to radiance factors by means of a different conversion. For want of better information, we have used a strict proportionality:

$$\rho = .03334 \ B \qquad\qquad (11)$$

and have compared the data so converted for several areas on the lunar surface, with the new photometric function. We find that the difficulty at large angles of incidence is almost entirely eliminated.

In Table II, we give the best values for compaction parameter and normal albedo for certain selected features of the lunar surface, and for comparison we also give where possible the compaction parameters for the same features as determined by Hapke.[1] Root mean square errors are also given where possible.

TABLE II

Compaction Parameters and normal albedoes for Selected Features
on the lunar surface.

Feature	Normal Albedo	Compaction Parameter g	r.m.s. error (Units of radiance factor)	g given by Hapke	Fedoretz Number
Maria	.081	.43	.0042	–	–
Terrae	.124	.625	.0054	–	–
Mountains below mare nectaris	.090	.65	.0020	.6	123
Mare Imbrium	.057	.46	.0035	.4	83
Bright ray in mare Serenitatus	.071	.24	.0024	.4	13
Near ray, Mare Serenitatus	.065	.18	.0031	.6	14
Clavius	.130	.76	.0103	–	97
Clomedes	.086	.59	.0044	–	10
Tycho	.133	1.03	.0167	.4	61
Pitatus	.069	.73	.0046	.6	96
Ptolmaeus	.081	.82	.0073	.6	52
Ocean of Storms	.050	.87	.0040	–	156
Ocean of Storms	.065	.50	.0038	–	161
Ocean of Storms	.053	.47	.0028	–	162

The wide dispority between compaction parameters determined using a Hapke retrodirective function, and the "new" retrodirective function, should be particularly noted. One should view with considerable caution predictions made about the actual porosity of the lunar surface on the basis of such calculations, since the values of the compaction parameter are so dependent on the model.

We have included in the table the available results for three positions within the ocean of storms, as that is the position of Surveyor I. We find an average compaction parameter for the ocean of storms of 0.62.

We note also that since our conversion, Equation (11) is strictly linear, the normal albedoes obtained by us will in general be somewhat lower than those tabulated by van Diggelen.

It is not difficult to determine the compaction parameters for a given lunar formation, provided photometric data as a function of i, ϵ and α are available. Van Diggelen's and Fedoretz' data are quite suitable for this. We have a computer program which, given any number of data points (less than 150), searches for the compaction parameter and normal albedo which gives the least squares fit with the data, using the new retrodirective function, Equation (8). This program is reproduced in Appendix IIC. The program also computes and prints a calculated value of the radiance factor for each

input value used in the least squares search. A sample of the output is also included in Appendix IIC.

Average Normal Albedo

Saari and Shorthill[6] give a statistical distribution of normal albedo from which a reasonably reliable average may be obtained. The resulting average is .095 which must be corrected, however, as the Saari-Shorthill data are adjusted to the brightness levels of Sytinskaya[7] which are too low. Orlova[3] has given corrections to Sytinskaya's values which on the average amount to an increase of 9.7%. Since Sytinskaya's average normal albedo is 0.098[8], the corrected normal albedo averaged for the whole moon is

$$\frac{.095}{.098} \times 1.097 = 0.106 \; .$$

This may be compared to the value 0.105 for the whole moon given by Russell.[8] Thus the measurements of the average normal albedo seem to be in agreement. In Table A-6 we have the energy from a lunar formation, integrated over all angles. The tables are for an assumed normal albedo of unity, for various compaction parameters and for various angles of incidence. Energies are in units of calories per squar centimeter per minute. Thus if the compaction parameter and normal albedo of a particular formation are known, the integrated energy of any angle of illumination may be found by looking up the energy given in the table for that value

of g and i, and then multiplying the entry by the normal albedo. For example, for Tycho at an angle of illumination of 60°, since the compaction parameter (from Table II) is 1.03, we find with interpolation an anergy entry of .611. Since the normal albedo is .133, the energy reflected into all angles under these conditions from Tycho should be .133 x .611 or .0812 cal/cm^{2}min.

When used in conjunction with tables of the energy conducted into the surface, quite accurate estimates of the integrated infrared radiant energy may be made from considerations of energy balance. For example, suppose we take for the whole moon an average normal albedo of .106, and an average compaction parameter of 0.51. Then the energy reflected from the subsolar point should be 0.0964 cal/cm^{2}min. The energy conducted into the surface at this point is .0103 cal/cm^{2}min, and there are no other important sources or sinks of energy. Therefore using 1.99 cal/cm^{2}min as the input energy from the sun, this leaves 1.88 cal/cm^{2}min which should be emitted in the form of heat radiation. Such values obtained by energy balance are probably in error by no more than 1.5%. We have adopted the value 1.88 cal/cm^{2}min from the subsolar point in our discussion of infrared energy in Chapter IV, in order to determine some of the adjustable parameters.[4]

Finally we note that the new photometric function, Equation (8), appears to approach zero a little too rapidly at angles of incidence near 90°. This is because of the factor

$s(i, \epsilon)$, which introduces an extra cosi into the numerator

making the brightness approach zero as $\cos^2 i$ for i near 90°.

From the overall point of view of the amount of energy

involved, this error is slight. However, it is an admitted

defect of the photometric function. A better photometric

function could be obtained--without any particular theoretical

justification--by replacing cosi in $s(i, \epsilon)$ by cosi+a; a is a

number of the order of 0.1. However we have not carried out

a detailed investigation of this.

Further slight improvements in the photometric function

may be made by modifying the scattering function $\sum(\alpha)$, in

Equation (6). However due to the scatter in the raw data,

and the crudeness in the model, it does not seem likely that

such efforts will lead to improved understanding of the

directional characteristics of lunar reflected radiation.

Conclusions

We have presented numerous numerical calculations based on a new photometric function, Equation (8), which depends on a complicated way an angle of incidence, angle of observation, and phase angle. The agreement with observations is much improved with respect to earlier photometric functions. A systematic error in the conversions of van Diggelen has been pointed out, leading to improved agreement between theory and observations at the larger angles of incidence. The resulting photometric function agrees satisfactorily with observations except for ϵ very near 90°, where the calculated radiance factors approach zero a little too rapidly.

One remaining problem is that a limited number of craters show a maximum in brightness a few degrees (in phase) after full moon, whereas all photometric functions discussed here have their maxima at full moon, $\alpha = 0$. We have no explanation for this. We mention again, finally, the poor correlation between values of the compaction parameter as determined using different photometric functions, which are yet based fundamentally on the same model of the surface. It is felt that, since the new photometric function agrees so much better with observations, that the values of the compaction parameters determined therefrom are more likely to be accurate than those determined using a Hapke function.

REFERENCES FOR CHAPTER II

1. B. W. Hapke, Journal of Geophysical Research 68, 4571 (1963).

2. V. A. Fedoretz, Utch. Zap. Kharkov Univ., 42, 49 (1952).

3. N. S. Orlova, Akad. Nauk, Astro. Zh. 33, 1 (1956).

4. N. Ashby, Publ. Astr. Soc. Pac. 78, No. 461, 254 (1966).

5. J. Van Diggelen, Recherches Astr. de l'Observ. d'Utrecht 14, No. 2 (1960).

6. Soari and Shorthill, Boeing Geoastrophysics Review, July-December, 1965, p. 38.

7. Sytinskaya, N.N., V. V. Sharonov, Uchen. Zap. Lening. UN-TA, No. 153, 114 (1952).

8. V. V. Sharonov, Nature of the Planets, NASA TTF-77, p.258 (1964).

9. H. N. Russell, Ap. J. 53, 114 (1916).

APPENDIX IIA

Comparison of Calculated and Observed Radiance Factors for Terrae and Maria using "new" Retrodirective Function.

Table A-1

Observed radiance factor ρ along equator for terrae (Orlova, 1956)

ϵ* i	0	10°	20°	30°	40°	50°	60°	70°	80°
80	.028	–	.042	.054	.057	.066	–	–	–
70	.036	.042	.048	.064	.067	.077	.095	.124	–
60	.043	.051	.054	.075	.077	.097	.124	.083	–
50	.051	.061	.063	.087	.095	.124	.086	.053	–
40	.061	.071	.076	.107	.123	.093	.058	.038	
30	.072	.086	.102	.124	.095	.064	.045	.030	–
20	.086	.102	.123	1.04	.070	.051	.036	.021	–
10	.102	.129	.106	.085	.057	.042	.029	.021	–
0	.124	.106	.083	.067	.047	.033	.024	.017	–
10	.102	.083	.068	.055	.041	.029	.020	.015	–
20	.086	.072	.058	.046	.035	.024	.017	.013	–
30	.072	.059	.050	.036	.028	.021	.015	.012	–
40	.061	.051	.044	.030	.024	.017	.014	.011	–
50	.051	.041	.035	.026	.021	.016	.013	.010	–
60	.043	.034	.030	.022	.018	.016	.012	.009	–
70	.036	.025	.023	.019	.017	.016	.012	.009	–
80	.028	.017	.016	.017	.015	.016	.012	.009	–

*The values of ϵ_1 from top to bottom, correspond to increasing phase from just after first quarter to just before last quarter.

TABLE A-2

Observed radiance factor ρ along equator for maria (Orlova, 1956)

ε i	0	10°	20°	30°	40°	50°	60°	70°
80°	.024	.033	.030	.029	.030	.031	—	—
70°	.026	.033	.034	.034	.036	.040	.056	.081
60°	.027	.034	.038	.040	.044	.055	.081	.044
50°	.030	.037	.041	.050	.057	.081	.053	.028
40°	.034	.041	.050	.065	.081	.057	.035	.019
30°	.040	.049	.061	.081	.058	.040	.026	.015
20°	.049	.062	.081	.061	.044	.031	.020	.012
10°	.066	.081	.061	.046	.034	.026	.016	.010
0°	.081	.069	.048	.035	.028	.021	.013	.008
10°	.066	.052	.039	.028	.023	.018	.011	.007
20°	.049	.041	.033	.025	.021	.015	.009	.006
30°	.040	.033	.029	.023	.018	.013	.009	.006
40°	.034	.030	.025	.022	.018	.011	.008	.005
50°	.030	.028	.023	.020	.015	.010	.008	.005
60°	.027	.026	.021	.018	.014	.010	.007	.005
70°	.026	.024	.021	.017	.012	.008	—	—
80°	.024	—	—	—	—	—	—	—

TABLE A-3

Calculated Radiance Factor ρ along Equator for Terrae (new retrodirective function, $g = .625$, $a = .124$).

ε \ i	0°	10°	20°	30°	40°	50°	60°	70°	80°
80°	.022	.026	.033	.040	.051	.066	.087	.115	.124
70°	.035	.044	.053	.064	.076	.092	.111	.124	.059
60°	.047	.055	.065	.077	.090	.108	.124	.077	.030
50°	.054	.064	.075	.088	.106	.124	.084	.049	.018
40°	.062	.072	.085	.104	.124	.089	.059	.034	.011
30°	.070	.083	.102	.124	.092	.065	.044	.025	.008
20°	.080	.100	.124	.094	.069	.051	.035	.019	.006
10°	.099	.124	.096	.073	.056	.042	.028	.015	.005
0°	.124	.097	.076	.060	.047	.035	.023	.012	.004
10°	.099	.078	.064	.052	.040	.030	.019	.010	.003
20°	.080	.067	.055	.045	.035	.025	.016	.008	.002
30°	.070	.059	.049	.039	.030	.021	.014	.007	.002
40°	.062	.052	.043	.034	.026	.018	.011	.005	.002
50°	.054	.045	.037	.029	.021	.015	.009	.004	.001
60°	.046	.038	.030	.023	.017	.012	.007	.003	.001
70°	.036	.029	.023	.017	.012	.008	.005	.002	.001
80°	.022	.017	.013	.010	.007	.004	.002	.001	–

TABLE A-4

Calculated Radiance factor ρ along Equator for Maria (new retrodirective function, $g = .372$, $a = .081$).

ϵ \ i	0°	10°	20°	30°	40°	50°	60°	70°
80°	.014	.017	.021	.026	.032	.040	–	–
70°	.023	.028	.034	.039	.046	.054	.066	.081
60°	.029	.035	.040	.046	.053	.064	.081	.045
50°	.034	.039	.045	.051	.062	.081	.050	.029
40°	.038	.043	.050	.061	.081	.052	.035	.021
30°	.042	.049	.060	.081	.054	.038	.027	.016
20°	.047	.059	.080	.055	.041	.031	.021	.012
10°	.058	.081	.056	.043	.034	.026	.018	.010
0°	.081	.057	.044	.036	.029	.022	.015	.008
10°	.058	.046	.038	.032	.025	.019	.012	.007
20°	.047	.040	.034	.028	.022	.016	.010	.005
30°	.042	.036	.030	.025	.019	.014	.009	.005
40°	.038	.032	.027	.022	.017	.012	.007	.004
50°	.034	.029	.024	.019	.014	.010	.006	.003
60°	.029	.024	.020	.015	.011	.007	.004	.002
70°	.023	.019	.015	.011	.008	.005	–	–
80°	.014	–	–	–	–	–	–	–

TABLE A-5

Average Integrated Energy (in $cal/cm^2 sec$) Reflected from Terrae and Maria as a Function of Angle of Incidence.

Angle of Incidence	Energy Reflected For Maria	Energy Reflected for Terrae
0°	.0708	.116
5°	.0706	.115
10°	.0699	.114
15°	.0688	.112
20°	.0672	.110
25°	.0652	.106
30°	.0627	.102
35°	.0598	.097
40°	.0565	.092
45°	.0526	.085
50°	.0484	.078
55°	.0436	.070
60°	.0383	.062
65°	.0325	.052
70°	.0262	.042
75°	.0193	.031
80°	.0121	.019
85°	.0048	.008
90°	0	0

TABLE A-6

Integrated Energy Reflected From Lunar Surface with Compaction Parameter g and Albedo = 1.00, in cal/cm^2min. Accuracy is $\pm$ 5%.

Angle of incidence i	Compaction Parameter g									
	.200	.300	.372	.400	.500	.625	.700	.800	.900	1.000
0	.837	.850	.874	.883	.906	.933	.950	.971	.991	1.010
5°	.836	.857	.871	.880	.903	.930	.947	.968	.988	1.007
10°	.827	.849	.863	.871	.894	.921	.938	.958	.978	.996
15°	.814	.835	.849	.857	.879	.905	.922	.942	.961	.979
20°	.796	.816	.829	.838	.859	.884	.900	.919	.938	.956
25°	.772	.792	.805	.813	.833	.857	.872	.891	.908	.925
30°	.744	.763	.774	.782	.801	.824	.838	.856	.872	.888
35°	.710	.727	.738	.746	.764	.785	.798	.815	.830	.845
40°	.671	.687	.697	.704	.720	.740	.752	.767	.782	.796
45°	.626	.641	.650	.656	.671	.689	.700	.714	.727	.740
50°	.576	.589	.597	.602	.616	.632	.642	.654	.666	.677
55°	.519	.531	.538	.543	.554	.568	.577	.599	.598	.608
60°	.457	.467	.473	.477	.487	.499	.506	.515	.524	.532
65°	.388	.396	.401	.405	.413	.422	.429	.436	.443	.450
70°	.313	.319	.323	.325	.332	.339	.344	.350	.355	.361
75°	.232	.236	.239	.241	.245	.250	.253	.257	.261	.265
80°	.145	.148	.149	.150	.153	.155	.157	.160	.162	.164
85°	.0585	.0587	.0588	.0589	.0597	.0606	.0612	.0621	.0631	.0640

APPENDIX IIB

Here we give the computer program which reads in photometric data, searches for the compaction parameter g for the least squares fit of the new photometric function to the data, then computes and prints calculated values of the radiance factor for each data point. The program is written in Fortran II, suitable for use on a CDC 3600 computer.

The data input consists of any number of data decks, in sequence, each data deck being prefaced by a name card of up to 28 letters, such as:

1MARIA*

with a 1 in the first column (for page eject) and an asterisk before column 30. Following the name card in each data deck is a card specifying the number of data points to be processed, and the sines of the lunar coordinates λ and β, respectively, of the particular lunar feature being analyzed. The format is specified in Format statement number 4. Then following are the data cards on which for each data point are given the phase angle, radiance, angle of incidence, and angle of observation (See Format statement number 6), in that order. Angles are read in degrees.

The output of a determination of compaction parameter consists first of three columns labelled B, G, and RMS, which comprise a printed record of the search for the best G. B is

the albedo, G the compaction parameter, and RMS is the root mean square deviation between calculated and observed radiances. The last figures in the three columns are the most accurate values. Following this are three more columns labelled PHASE, BCAL, BOBS, which are the phase angle, calculated radiance, and observed radiance, respectively, for the best values of albedo and compaction parameter.

An end-of-file card follows the last data deck.

The program is written in six cycles of search, which gives somewhat less than 1% accuracy. If more accuracy is desired, the IF statement #101 may be modified by changing the 6 to whatever integral number of cycles is desired.

The new photometric function is contained in a Function subprogram (Statement 40 plus 3) which may easily be modified for use with other photometric functions.

APPENDIX IIC

COMPUTER PROGRAM FOR COMPUTING
COMPACTION PARAMETER FOR LEAST SQUARES DATA FIT

```
       PROGRAM LUN108A
C      COMPUTES PARAMETER FOR MINIMUM DEVIATION OF THEORETICAL PHOTOMET-
C      RIC FUNCTION FROM DATA, MAXIMUM NUMBER OF DATA POINTS IS 150
       DIMENSION ALPH(150),BBCAL(150),BOBS(150),BCAL(150),AINC(150),
      2AOBS(150),CINC(150),COBS(150),S(150),B1(150),B2(150),T(150),RMS(15
      30)
       COMMON/BLOCK1/BOBS,BCAL,B1,B2,S.T,DD,RT,B,G,M
1      FORMAT(*                                    *)
4      FORMAT (I3,2F6.3)
6      FORMAT (F7.1,F7.3,2F6.3)
7      FORMAT (*    B            G          RMS*)
14     FORMAT (3F10.5)
15     FORMAT (F7.1,2F7.4)
105    READ 1
       IF (EOF,60)2,3
2      CALL EXIT
3      READ 4, M, SILAM, SIBET
       DO 5 I = 1,M
5      READ 6, ALPH(I), BOBS(I), AINC(I), AOBS(I)
       PRINT 1
       PRINT 7
       M1 = M+1
       DO 8 I = M1, 150
       BOBS(I) = 0.0
8      BCAL(I) = 0.0
       C = 3.14159/180.0
       DO 9 I = 1,M
       COBS(I) = COSF(C*AOBS(I))
9      CINC(I) = COSF(C*AINC(I))
       DO 10 I = 1,M
       B1(I) = 4.0*COBS(I)*(CINC(I)**2)/((COBS(I)+CINC(I))**3)
       AL = ABSF(ALPH(I))
       B2(I)= ((3.14159-C*AL)*COSF(C*AL)+SINF(C*AL))/3.14159
       S(I) = 0.5*(COBS(I)+CINC(I))*((1./COBS(I))+(1./CINC(I)))
10     T(I) = TANF(C*AL)
       DD = 0.0
       DO 51 I = 1,M
51     DD = DD + (BOBS(I))**2
       N = 1
       J = 1
       DELG = 0.1
       G = 0.5
       DO 37 I = 1,M
37     BCAL(I) = ENERGYF(B1(I),B2(I),S(I),T(I),G)
       CALL RTMS
       RMS(J) = RT
       J = J+1
       PRINT 14, B,G,RT
100    G = G+DELG
       DO 38 I = 1,M
```

```
38      BCAL(I) = ENERGYF(B1(I),B2(I),S(I),T(I),G)
        CALL RTMS
        RMS(J) = RT
        J = J+1
        PRINT 14, B,G,RT
        IF(RMS(J-1)-RMS(J-2)) 100,101,101
101     IF(N-6) 104,102,102
104     DELG = -DELG/2.718282
        N = N+1
        GO TO 100
102     CONTINUE
        DO 39 I = 1,M
39      BBCAL(I) = B*BCAL(I)
47      PRINT 48
48      FORMAT(* PHASE      BCAL      BOBS*)
        DO 40 I = 1,M
40      PRINT 15, ALPH(I), BBCAL(I), BOBS(I)
        GO TO 105
        END
        FUNCTION ENERGYF (B1,B2,S,T,G)
        IF (T) 61,62,62
61      B3 = 1.0
        GO TO 63
62      E = EXPF(-.5*G*S/T)
        B3 = 2.0 - .5*T*(1.-E)*(3.-E)/G + (.5*S-1.)*E*(2.-E)
63      ENERGYF = B1*B2*B3
        RETURN
        END
        SUBROUTINE RTMS
        DIMENSION BOBS(150),BCAL(150),B1(150),B2(150),S(150),T(150)
        COMMON/BLOCK1/BOBS,BCAL,B1,B2,S,T,DD,RT,B,G,M
        DF = 0.0
        DO 11 I = 1,M
11      DF = DF + BOBS(I)*BCAL(I)
        FF = 0.0
        DO 12 I = 1,M
12      FF = FF+BCAL(I)**2
        B = DF/FF
        RT = DD - (B**2)*FF
        RT = SQRTF(RT/FLOATF(M))
        RETURN
        END
```

SAMPLE OUTPUT FROM SEARCH PROGRAM LUN108A

Pitatus*

B	G	RMS
0.07371	0.50000	0.00467
0.07132	0.60000	0.00463
0.06942	0.70000	0.00461
0.06788	0.80000	0.00461
0.06841	0.76321	0.00461
0.06899	0.72642	0.00461
0.06960	0.68964	0.00461
0.06937	0.70317	0.00461
0.06914	0.71670	0.00461
0.06892	0.73024	0.00461
0.06871	0.74377	0.00461
0.06879	0.73879	0.00461
0.06887	0.73381	0.00461
0.06895	0.72883	0.00461
0.06903	0.72386	0.00461
0.06900	0.72569	0.00461
0.06897	0.72752	0.00461
0.06894	0.72935	0.00461
0.06891	0.73118	0.00461
0.06892	0.73051	0.00461
0.06893	0.72983	0.00461
0.06894	0.72916	0.00461

Phase	BCAL	BOBS
11.4	0.0558	0.0619
23.9	0.0424	0.0494
77.9	0.0074	0.0130
91.3	0.0018	0.0116
-77.5	0.0001	0.0007
-72.0	0.0020	0.0017
-64.2	0.0053	0.0050
-61.7	0.0026	0.0100
-50.9	0.0139	0.0150
-50.3	0.0111	0.0153
-39.5	0.0227	0.0243
-28.3	0.0338	0.0330
-25.7	0.0377	0.0333
-17.6	0.0454	0.0407
-11.3	0.0536	0.0450
-8.9	0.0562	0.0546
-7.1	0.0625	0.0546
-1.5	0.0670	0.0710

SAMPLE OUTPUT FROM SEARCH PROGRAM LUN108A

Pitatus*

Phase	BCAL	BOBS
4.6	0.0635	0.0597
5.5	0.0632	0.0637
13.1	0.0542	0.0630
17.8	0.0480	0.0520
23.0	0.0437	0.0410
42.4	0.0266	0.0297
50.2	0.0217	0.0216
57.3	0.0186	0.0150
62.6	0.0135	0.0116
73.5	0.0072	0.0100
79.9	0.0055	0.0096
82.1	0.0034	0.0050
96.4	0.0003	0.0007

CHAPTER III

DERIVATION OF PHOTOMETRIC FUNCTIONS

Introduction

In this chapter our purpose is to derive a law describing the light reflected from an element of the lunar surface. We shall assume the reader is familiar with the basic ideas of reflection, scattering, and brightness.

A reasonably good mathematical expression for the photometric properties of the lunar surface has been obtained by Hapke.[3] The model on which his derivation is based consists of a semi-infinite, porous layer of randomly placed obscuring objects suspended in depth in such a way that the interstices separating them are interconnected.

We shall not repeat the derivation at this point since it is discussed and extended later in this report. The resulting expression for the reflected energy, $I^{(re)}(i,\epsilon,\alpha)$ per unit solid angle per unit time from a unit area of actual lunar surface, when the solar insolation is incident at angle i from the mean surface normal and the reflected radiation is observed at angle ϵ from the mean surface normal, with α the angle between incident and observation directions, is as follows:

$$I^{(re)}(i,\epsilon,\alpha) = S_o \frac{\cos \epsilon \cos i}{\cos i + \cos \epsilon} b \sum(\alpha)B(\alpha,g) \qquad (1)$$

where S_o is the solar constant, and b is the total reflectivity of an object, i.e., the fraction of incident light reflected by

the object into all directions. The function $\sum(\alpha)$ is the scattering law of an individual object. In his work, Hapke uses the backscattering expression

$$\sum(\alpha) = [(\pi-\alpha)\cos\alpha +\sin\alpha]/\pi \qquad (2)$$

which satisfies the normalization condition

$$\overline{\sum}(0) = 1 \qquad (3)$$

and corresponds to an opaque spherical particle diffusely reflecting from the illuminated portion of its surface.

The function $B(\alpha,g)$ expresses the effect of shadowing on the porous surface. Hapke gives the following expression for this so-called "retrodirective function":

$$B(\alpha,g) = \begin{cases} [2-\tan\alpha(1-e^{-g/\tan\alpha})/2g](3-e^{-g/\tan\alpha}), & \alpha \le \pi/2 \\ 1 & \alpha > \pi/2 \end{cases}$$

$$(4)$$

where g is a parameter related to the degree of porosity of the lunar surface material, or to the fraction of void space at the surface. The parameter g may vary from place to place on the surface; Hapke obtains most of his good fits with experimental data by choosing

$$g = 0.6 \qquad . \qquad (5)$$

However, g may vary from 0.4 to 0.8. The best average value
for g using Equation (4) the whole moon seems to be g $\simeq$ 0.7.

The parameter b may also vary from place to place; it is
determined from the albedo at the particular location of interest.

These expressions, with proper choice of multiplication
factor b, represent reasonably well the observed photometric
properties of the moon. At large angles of incidence and at
large phase angles, the observed reflected light is greater
than that predicted by Equation (1).

We now ask, how can we improve the expression (1)? We
note that basically the model gives rise to a result which is
the product of three factors; there are first the Lommel-Seeliger
law,

$$\frac{1}{1 + \cos \epsilon / \cos i}$$

which insures that $I^{(re)}$ = 0 when i = 90°, secondly, the scatter-
ing law $\sum(\alpha)$ and thirdly the shadowing function $B(\alpha, g)$. We shall
now consider possible modifications of Hapke's argument which
will still allow $I^{(re)}$ to be written as a product of the
same three factors. We are mainly interested in modifications
of the retrodirective function $B(\alpha, g)$.

The Retrodirective Function

If one looks at the detailed physical model implied in
Hapke's treatment,[3] one sees that the rectangular tubes repre-
senting the incident light are truncated at right angles to the
beam. These tubes are then oriented so that one edge is per-
pendicular to the plane formed by the incident ray and the
direction of observation. This simplification is made in order
that the area seen at the base of the cylinder is a simple
rectangle and not a triangle or a four-sided figure as it
would be if the incident square cylinder of light were trun-
cated by the mean lunar surface. Actually, the incident
cylinder of light is not truncated by the mean lunar surface,
but rather by the surface of the facet upon which it is incident.
In Hapke's treatment he introduces the mean lunar surface as a
reference plane when actually one should treat the face of the
facet itself as a reference plane. It would be a good approx-
imation to use the mean lunar surface as a reference plane if
the penetration of the light into the material were large
compared with the dimensions of the reflecting particles or
elements in the medium. This is not the case, however, since
Hapke found that the penetration depth is approxmately equal to
the diameter of the reflecting particles in the mediu. He ob-
tained best fit with experiment when the ratio $g = (a/\tau) \simeq 1$.
a is the diameter of the particles and τ the attenuation dis-
tance, that is, the distance over which radiation decreases to
1/e of its initial value. A literal interpretation of Hapke's

model would be one in which all facets were normal to the direction of the incident beam. If this were the case, then the distance over which the light is attenuated on its way out should be measured to that surface. Such a surface would be simply an extension of the surface end of the square cylinder. Hapke extends the path of the reflected rays to the mean lunar surface.

A literal interpretation of the model, however, may not ignore the details of the geometry of the light cylinders at the surface and the change in path length in the absorbing medium associated with those details. We expect the substratum for which such particles form a surface layer to be much larger than the particles themselves. Therefore, it is not proper to write $z\cos i = z'\cos \epsilon = y$ as does Hapke (Figure 2). This does not conform to Hapke's notation; in Figure 2, z is the path length of the light as it enters the medium measured to the point at which a reflection (scattering) occurs and z' is the distance from the reflecting particle to the lunar surface. Measuring these lengths to the lunar surface enables Hapke to introduce the angle of incidence, i, of the incoming light. i is the angle which the incoming light makes with a normal to the lunar surface (mean lunar surface). ϵ is the angle of observation measured from the normal to the lunar surface. The above relation is the key equation leading to the Lommel-Seeliger law.

If the dimensions of surface facets are large compared with
τ, then i and ϵ should be replaced by i' and ϵ', where the latter
are measured with respect to a normal to the facet itself rather
than the normal to the lunar surface.

One may completely generalize the problem (with the re-
striction that the reflecting elements in the medium are regarded
as small squares) by letting the facet upon which the light is
incident truncate the incident cylinder in a completely arbitrary
manner. One of the difficulties that enter into the details of
this model is the problem of deriving a simple expression for the
area of the bottom of the cylinder as seen by an observer. The
details of this calculation are now largely completed but the
expressions are algebraically too complicated to permit calcula-
tions to be made for inclusion in this report. In the calculations
referred to, the incident square cylinder of light is truncated in
an arbitrary direction by the surface of the facet. The visible
area, the non-visible area, the incident path length, and
exiting path length are expressed in terms of angles i' and ϵ'
which define the direction of incidence and the direction of
viewing with respect to a normal to the facet. After a general
expression for the intensity of the emergent beam is obtained
for a particular facet, one must introduce a reference line
normal to the mean lunar surface and average final results over
all orientations of the facets. Since the direction of the in-
cident beam and the reflected beam are specified in an absolute

sense, the angle between the incident beam $\hat{n}_i$ and the direction

of the reflected beam $\hat{n}_o$ will be the same as the angle between

$\hat{n}_i'$ and $\hat{n}_o'$ where the primes merely designate that the directions

of these rays are defined with respect to a normal to the facet.

When unprimed, it is understood that their orientation is defined

with respect to the mean lunar surface. The algebra required

to relate results for an arbitrary facet and involving angles

i' and ϵ' to a final expression involving i and ϵ plus an

additional angle and then averaging over all values of this

angle is not yet completed but the procedure is clear. Addition-

al time will be required to complete the details and perform

calculations. We, therefore, return to the simpler picture of

Hapke and treat his model more realistically. The purpose of

pursuing such details is to attempt to establish a range of

flexibility in the final results. One will then know how much

he can tamper with the theoretical curves in order to obtain

best agreement with experiment.

For simplicity in calculating the visible area at the bottom

of the light cylinder, we shall now follow Hapke in orienting the

cylinder so that one edge is perpendicular to the plane formed by

the incident ray and the reflected ray. We shall first regard

the surface facet as being always normal to the incident beam.

In general, the facets will be oriented in all possible direc-

tions. We can introduce only one degree of freedom in the orien-

tation of the facets which is consistent with keeping an edge of

the cylinder perpendicular to the plane of $\hat{n}_i$ and $\hat{n}_o$ and that is

to allow the surface to rotate about the line at the top of the

cylinder and perpendicular to the plane of $\hat{n}_o$ and $\hat{n}_i$. This angle

is designated by β in Figure 6. The distance the light travels

before hitting the reflecting elements at the bottom of the

cylinder is z as shown in Figure 6. We now differ from Hapke

in that the reflected light will attenuate as it travels from the

bottom of the cylinder to the extension of the plane of the

facet as shown in the figure. It is obvious that the geometry

of this treatment will involve neither i nor ϵ, but will be de-

pendent only upon α. As another refinement, not that the re-

flected light does not start to attentuate, that is, it does not

encounter absorbing medium until it crosses the wall of the

cylinder. For simplicity the exiting path of the seen area is

measured from the edge of the area, but this detail is not im-

portant here since no attenuation factor along the path is

introduced in this case. We will consider the following cases:

1. Truncate the incident cylinder perpendicular to the

incident beam.

(a) Measure the path of the light scattered from

the unseen area from the edge of the area to the surface of

the facet. Introduce the exponential attenuation factor independ-

ently of whether the line is inside or outside the cylinder.

(b) Modify the above procedure by measuring the attenuation path from the midpoint of the unseen area and also take into account that attentuation does not begin until the rays intersect the side of the cylinder.

2. Allow the surface facet to make an angle β with the plane perpendicular to the normal of the incident beam. Introduce the exponential attenuation factor independently of whether the line is inside or outside of the cylinder.

Measure the path of the light reflected from the unseen area to the middle of the area and introduce attenuation only after it leaves the side of the cylinder. Measure incoming attenuation path to midpoint of seen area. Average over all β.

The above procedures will then yield different forms for the function $B(\alpha)$. Hapke calls this function the retrodirective function. As we shall see, our procedure will modify Hapke's results to the extent of obtaining different retrodirective functions. Differences among these cases may be minor; nevertheless, formulas for each have been derived. We shall see that a modification of 1(a) gives Hapke's retrodirective function.

The angles i and ϵ enter Hapke's expression through the Lommel-Seeliger law which appears as a separate factor multiplying the function $B(\alpha)$. In order to make formulas satisfy the reciprocity condition, Hapke makes the substitution

$$\sec i \simeq (\sec i + \sec \epsilon)/2.$$

Since i and ϵ do not enter our description when deriving the retrodirective function, we now ask how they should be introduced. It is reasonable to introduce them as follows: first let us suppose that the average slope of the facets coincides with the mean lunar surface. It then appears reasonable to say that, on the average, a large ϵ will introduce a longer attentuation path in the absorbing medium than would a small ϵ. We will therefore now regard the lunar surface as flat. We assume that on the average one can write $z \cos i = z' \cos \epsilon = y$, where z, z' and y are defined in Figure 2. One then derives the Lommel-Seeliger law in the usual manner, and uses it to modulate the function $B(\alpha)$. Note that this plausibility argument satisfies the reciprocity theorem. It may also be mentioned here that the general results wherein the incident cylinder is truncated in an arbitrary manner by a facet and then averaged over all orientations of facets do not satisfy the reciprocity theorem. In that case then, one must arbitrarily introduce reciprocity through the substitiution $\sec i = (\sec i + \sec \epsilon)/2$ as does Hapke. It is therefore not clear that the results obtained from arbitrary truncation will be any more significant than the results obtained in the present model, since the more general results have to be doctored up to satisfy reciprocity.

Before proceeding to a detailed calculation of $B(\alpha)$ in our model, we first derive the Lommel-Seeliger law, and also review the derivation of Hapke's formulas.

Derivation of Exponential Absorption Factor

In the following discussion we regard a plane wave of light as incident upon a material made up of randomly distributed scattering elements. Suspended particles of dust would satisfy this model if the particles were kept separated from each other by electrostatic forces. When light encounters a particle, it will be scattered in the angle range $d\alpha$ as specified by a scattering function $b(\alpha)$. Above the particle there is effectively an empty tube reaching to the surface out of which some light can escape with zero probability of a collision with another particle.

If the reflected light crosses the side of this imaginary tube before reaching the surface, then there will be a finite probability of encountering another particle in the medium before the light escapes from the medium.

If B_o is the area of the plane wave of light at the surface of the medium, and S_o the energy flux per unit area of the beam incident at angle i with respect to the normal of the surface, then $S_o B_o e^{-n_o a_o z} = S_o B_o e^{-z/\tau}$ is the energy entering lunar surface of area $B_o/\cos i$ which has not yet been scattered after beam travels a distance z along the path beneath the surface. This may be seen as follows. Let B be the cross section of incident beam at any depth z. Let $a_o = a^2$ be the area of intercepting elements and n_o the number of such elements per unit volume. Tubes of light are shown schematically in Figure 3. The decrease in the area of the beam (that is, the portion scattered) in traveling distance dz is:

$$dB = -n_0 a_0 B dz$$

$$B = C e^{-n_0 a_0 z}.$$

Therefore, area of beam at surface is B_0 so that:

$$B = B_0 e^{-n_0 a_0 z}.$$

Thus energy scattered out of beam in distance dz (layer dy) (Figure 2) is

$$B_0 S_0 n_0 a_0 e^{-n_0 a_0 z} dz = B_0 S_0 n_0 a_0 e^{-\frac{n_0 a_0 y}{\cos i}} \frac{dy}{\cos i}$$

since $dz = dy/\cos i$. This energy is incident over an area of lunar surface $B_0/\cos i$. So energy incident over unit surface area and scattered out in distance z is $S_0 n_0 a_0 e^{-n_0 a_0 y/\cos i} dy$. The energy scattered per unit volume (since volume of scattering region is $\frac{B_0}{\cos i} \times dy$) is $S_0 n_0 a_0 e^{-n_0 a_0 y/\cos i}$. Therefore $S_0 n_0 a_0 e^{-n_0 a_0 y/\cos i}$ is the energy produced per unit volume of scattering material per unit solid angle. If there is some pure absorption then only a fraction (say f_0) of this energy will be scattered.

If we neglect that part of the path length which is in the empty tube and consider the light which hits a scattering center as again traveling through the same medium and therefore having

a probability of being scattered again before reaching the
surface, we can write:

$$dB = -n_o a_o B dz'$$

$$B = B' e^{-n_o a_o z}$$

since $B = B'$ when $z' = 0$. Thus the fraction of light scattered
at $z' = 0$ which gets out after traveling distance z' is
$e^{-n_o a_o z'} = e^{-n_o a_o y / \cos \epsilon}$.

In the above discussion we have omitted the scattering
function $b(\alpha)$ since it depends only on α and not z or z'. We
will now let $n_o a_o = 1/\tau$ where τ is the mean attenuation length
of a beam of light rays in the medium. If the particles are
far apart (average distance apart large compared with diameter
of particles) then $\tau = 1/n_o a_o$ exactly. If the objects are
close together, shielding of one object by another will be
common so that each object is less efficient at blocking
light and hence $\tau > 1/n_o a$.

Lommel-Seeliger Scattering Law

The energy leaving a volume of thickness dy and unit area
is $f_o \frac{S_o}{\tau} \exp \frac{-y}{\cos i} dy$. Multiplying this by the fraction $e^{-y/\tau \cos \epsilon}$
which reaches the surface, we obtain for the energy leaving per
unit solid angle per second from a unit area of surface:

$$\int_{y=0}^{\infty} \frac{f_o S_o e^{-y/\tau \cos i}}{\tau} e^{-y/\tau \cos \epsilon} dy$$

$$= f_o S_o \left[\frac{1}{\frac{1}{\cos \epsilon} + \frac{1}{\cos i}} \right]$$

Energy out per unit area of surface
$$= f_o S_o \left[\frac{\cos i \cos \epsilon}{\cos i + \cos \epsilon} \right] . \qquad (6)$$

This is the Lommel-Seeliger law.

In terms of the brightness this energy is expressed as $B(i, \epsilon) \cos \epsilon$. Thus:

$$B(i, \epsilon) = f_o S_o \frac{\cos i}{\cos i + \cos \epsilon} . \qquad (7)$$

The brightness is the energy through a unit area perpendicular to the direction of observation.

The size of a unit area of lunar surface projected perpendicular to direction of observation is $\cos \epsilon$. Therefore, we divide (6) by $\cos \epsilon$ to obtain flux per unit area. Equation (7) must be multiplied by the projected lunar area seen by the detector and also multiplied by the solid angle subtended by the detector as seen from the lunar surface.

Derivation of Hapke's Results

The general features of Hapke's model have already been described. Hapke points out that an observer looking along line O'P (see Figure 4) will only see part of the area of the bottom of the cylinder. Referring to Figure 4 the viewed area is given by $A = a(a-x)$ where $x = z \tan \alpha$. As mentioned earlier, Hapke now writes

$$z \cos i = z' \cos \epsilon = y \qquad (8)$$

so that the exiting ray is measured to the lunar surface. If one goes along with this, we can now write

$$A = a(a - z\tan\alpha) = a^2 - az'\cos\varepsilon\,\tan\alpha\,/\cos i$$

$$A = a^2 - ay\,\sec\,i\,\tan\,\alpha$$

From this the seen fraction $F = A/a^2$ of the total area A is :

$$F = A/a^2 = 1 - y(\sec\,i\,\tan\,\alpha)/a = 1 - \frac{x}{a} \tag{9}$$

The fraction of the area which cannot be seen directly is:

$$1 - F = \frac{x}{a}$$

where

$$\frac{x}{a} = y\,(\sec\,i\,\tan\,\alpha)/a$$

The expression for F is not symmetrical in i and ε. In order to make it symmetrical in i and ε Hapke then makes the substitution $\sec\,i \simeq (\sec\,i + \sec\,\varepsilon)\,/2.$

Thus

$$\frac{x}{a} = y(\,\sec\,i\,\tan\alpha\,)/a = y\,(\sec\,i + \sec\,\varepsilon\,)(\tan\alpha\,)/2a$$

with this substitution our Equation (9) for F becomes

$$\frac{A}{a^2} = F - 1 - y \, (\sec i + \sec \epsilon)(\tan \alpha)/2a$$

$$= 1 - \frac{z'}{2a} \left(\frac{\cos \epsilon}{\cos i} + 1 \right) \tan \alpha \qquad (10)$$

This expression for F is the same as Hapke's except that in his notation, his x is our x/a and his y is our a/2. For a given α, A becomes zero for $z > z_o$ where $z_o \tan \alpha = a$; $z_o = a \cot \alpha$. Multiplying the seen area by the exponential attenuation factor $e^{-z/\tau}$ and the unseen area by $e^{-(z+a')/\tau}$, one obtains

$$\int_o^{z_o} A e^{-z/\tau} \, dz' + \int_o^{z_o} (a^2-A) e^{-(z+z')/\tau} \, dz' + a^2 \int_{z_o=a \cot \alpha}^{\infty} e^{-(z+z')/\tau} \, dz' \qquad (11)$$

Hapke makes use of the relation:

$$z \cos i = z' \cos \epsilon = y$$

so that

$$e^{-z/\tau} = e^{-z' \cos \epsilon /\cos i} = e^{-y \sec i/\tau}$$

and

$$e^{-z+z')/\tau} = e^{-z'(1+\frac{\cos \epsilon}{\cos i})/\tau} = e^{-y(\frac{1}{\cos \epsilon} + \frac{1}{\cos i})/\tau}$$

Equation (11) can be written in terms of xz' as:

$$\int_o^{z_o} A e^{-z' \cos \epsilon \, \sec i} \, dz' + \int^{\infty} (a^2 - A) e^{-z'(1\frac{\cos \epsilon}{\cos i})/\tau} \, dz'$$

Where the first integral is now 0 to ∞ rather than 0 to z_o

but we specify A = 0 for z > z_o. Putting sec i $\simeq$ (sec i + sec ε)/2

in the first exponential: (but not the second)

$$\int_0^{z_o} A e^{-z(\frac{\cos \epsilon}{\cos i} + 1)/2\tau} dz' + \int_0^{\infty} (a^2 - A) e^{-z'(1 + \frac{\cos \epsilon}{\cos i})/\tau} dz' \qquad (12)$$

This is now reversible when we use (10) for area A, that is,

the exact A with the substitution sec i $\simeq$ (sec i + sec ε)/2.

The exponential in the second integrand when written

in the form $y(\frac{1}{\cos \epsilon} + \frac{1}{\cos i})$ is symmetrical in ε and i. The

exponential of the first integrand, $e^{-y \sec i/\tau}$, is made symmetrical

in i and ε by the substitution sec i = (sec i + sec ε)/2.

Expressing the integrals in 4-26 in terms of y one has

letting $a^2 B$ be the sum of the integrals:

$$a^2 B = a^2 \int_0^{y_o} \{ 1 - \frac{y}{2a}(\frac{1}{\cos i} + \frac{1}{\cos \epsilon}) \tan\alpha \} e^{-y(\frac{1}{\cos \epsilon} + \frac{1}{\cos i})/2\tau} \frac{dy}{\cos \epsilon}$$

$$+ a^2 \int_0^{y_o} \frac{y}{2a}(\frac{1}{\cos i} + \frac{1}{\cos \epsilon}) \tan\alpha \; e^{-y(\frac{1}{\cos \epsilon} + \frac{1}{\cos i})/\tau} \frac{dy}{\cos \epsilon}$$

$$+ a^2 \int_{y_o}^{\infty} e^{-y(\frac{1}{\cos i} + \frac{1}{\cos \epsilon})/\tau} \frac{dy}{\cos \epsilon} \qquad (13)$$

Equation (13) divided by $\dfrac{a^2}{\cos\epsilon}$ yields the light exiting per unit area of scattering cross section parallel to the lunar surface. Dividing simply by a^2 yields the light exiting per unit area perpendicular to the direction of exit. The latter measure is directly related to the brightness which is the quantity seen by a detector scanning the lunar surface. We will therefore divide by a^2. In discussing reversibility, however, one must divide by $a^2/\cos\epsilon$, since energy is reversible, not the brightness. This will eliminate the $1/\cos\epsilon$ factor in Equation (13). Except for this factor, the integrand in Equation (13) is reversible, that is, unchanged with respect to an interchange of i and ϵ. The area factors in both integrals have already been symmetrized in i and ϵ by the substitution sec $i \approx (\sec i + \sec\epsilon)/2$.

Note that $y = z'\cos\epsilon$. Therefore $y_0 = z_0\cos\epsilon$. Now $y_0 = a\cot\alpha\cos\epsilon$. Thus although the integrand is invariant under an exchange of i and ϵ, the limit in y_0 is not invariant. We therefore replace $\cos\epsilon$ in the limit by $\dfrac{\cos\epsilon + \cos i}{2}$, so $y_0 = \ell a\cot\alpha$, where $\ell = \dfrac{\cos\epsilon + \cos i}{2}$.

We now carry out the integration with the integrand expressed in terms of y:

Let $1/\cos\epsilon + 1/\cos i = b$. The net expression is the form

3-19

$$a^2 \int_0^{y_o} \left(1 - \frac{by}{2a} \tan\alpha\right) e^{-by/2\tau} dy + a^2 \int_0^{y_o} \frac{by}{2a} \tan\alpha \; e^{-by/\tau} dy + a^2 \int_{y_o}^{\infty} e^{-by/\tau} dy$$

$$(14)$$

Now:

$$\int_0^{y_o} e^{-\frac{by}{2\tau}} dy = \frac{2\tau}{b}\left(1 - e^{-\frac{by_o}{2\tau}}\right)$$

$$-\frac{b}{2a}\tan\alpha \int_0^{y_o} y e^{-\frac{by}{2\tau}} dy = -\frac{b}{2a}\tan\alpha\left[-\frac{y_o 2\tau}{b} e^{-\frac{by_o}{2\tau}} + \frac{4\tau^2}{b^2}\left(1 - e^{-\frac{by_o}{2\tau}}\right)\right]$$

$$\frac{b\tan\alpha}{2a} \int_0^{y_o} y e^{-\frac{by}{\tau}} = \frac{b}{2a}\tan\alpha\left[-\frac{y_o \tau}{b} e^{-\frac{by_o}{\tau}} + \frac{\tau^2}{b^2}\left(1 - e^{-\frac{by_o}{\tau}}\right)\right] + \int_{y_o}^{\alpha} e^{-\frac{by}{\tau}} dy = \frac{\tau}{b}e^{-\frac{by_o}{\tau}}$$

$$+\int_{y_o}^{\alpha} e^{-\frac{by}{\tau}} dy = \frac{\tau}{b}e^{-\frac{by_o}{\tau}}$$

Collecting terms:

$$B\cos\epsilon = \frac{\tau}{b}\left\{2 - \frac{3\tau\tan\alpha}{2a} + \left[-2 + b\ell + \frac{2\tau\tan\alpha}{a}\right]e^{-by_o/2\tau} + \left[1 - \frac{b\ell}{2} - \frac{\tau\tan\alpha}{2a}\right]e^{-by_o/\tau}\right\}$$

$$(15)$$

Now $b = 1/\cos\epsilon + 1/\cos i$ and $\ell = \cos\epsilon + \cos i/2$ so $b\ell = \frac{1}{2}\left(1 + \frac{\cos i}{\cos\epsilon}\right)\left(\frac{\cos\epsilon}{\cos i} + 1\right)$.
Using the implication of Hapke's symmetrizing substitution that
$\cos i \approx \cos\epsilon$, $b\ell = 2$ and $b\cos\epsilon = 2$, one obtains

$$= \frac{\tau}{2}\left\{2 - \frac{3\tau}{2a}\tan\alpha + \frac{2\tau}{a}\tan\alpha\, e^{-\frac{a}{\tau\tan\alpha}} - \frac{\tau}{2}\tan\alpha\, e^{-\frac{2a}{\tau\tan\alpha}}\right\}. \qquad (16)$$

We now compare this with Hapke's formula 4-31 reference 3. Hapke writes

$$B(\alpha,g) = 2 - \frac{\tan\alpha}{2y}(1-e^{-y/\tan\alpha})(3-e^{-y\tan\alpha}) \qquad (17)$$

$g = \frac{2y}{\tau} = \frac{a}{\tau}$. Hapke's y is our $a/2$. In our notation, y is the vertical distance of a scattering point below the mean lunar surface.

Multiplying out Hapke's expression (17) and substituting $g = a/\tau$ we obtain

$$B(\alpha,g) = 2 - \frac{3\tau \tan\alpha}{2a} + \frac{2\tau}{a}\tan\alpha \, e^{-a/\tau \tan\alpha} - \frac{\tau \tan\alpha}{2a} e^{-\frac{2a}{\tau \tan\alpha}} \, .$$

(18)

Expression (18) of Hapke agrees with our derivation of his result, Equation (16).

We now modify Equation (15) in a plausible way in order to obtain a formula which gives quite good agreement with experimental data. We first note that (15) was obtained by introducing the symmetrizing substitutions $1/\cos i = \frac{1}{2}(1/\cos i + 1/\cos \epsilon)$. This implies that the formula should be valid when $\cos i \simeq \cos \epsilon$. This is only true for small values of i and ϵ. i and ϵ can differ from each other by large percentages but the cosines of each well only differ slightly if the angles are small. The quantities b1 and $by_0 (=b1 \, a \cot \alpha)$ in Equation (15) are slowly varying functions of i and ϵ. i and ϵ can differ from each other many fold while b1 will remain essentially constant. For example when $i = o$ and $\epsilon = o$, $b1 = 2$. When $i = o$ and $\epsilon = 45°$ $b1 = 2.05$. The one factor in Equation (15) which is not consistent with the symmetrizing substitution is the factor $1/b$. $1/b$ is the Lommel-Seeliger factor and in that sense should be present. The Lommel-Seeliger factor, however, is much more sensitive to large differences between i and ϵ. In the spirit of the derivation however, the formula should only be valid for $i \simeq \epsilon$. It may be used for a wide range of values of i and ϵ for which this

condition is not true if the function is relatively insensitive to values of i and ϵ. On the basis of this requirement we will replace 1/b cos ϵ by 1/b1 when writing an expression for B. Since b1 as well as b cos ϵ equals 2 when i = ϵ this gives Hapke's formula (16) for B. Thus we now end up with an expression for B, which happens to be symmetrical in i and ϵ although this is not required.

Referring to the starting Equation (11) we note that the first integral, which is a large term, shows no attenuation of the light as it leaves the cylinder after being scattered by the seen area of the base. Putting Hapke's symmetrizing condition in the exponential is equivalent to introducing attentuation, on the way out of the cylinder (except that the attentuation factor is only half of what it would be if true attentuation were taking place). The two remaining integrals contain attenuation terms for light entering the medium as well as for light leaving the medium. One might say that the final 1/b factor (Lommel-Seeliger law) enters legitimately from this part of the total Equation (11) (Area A is still symmetrized artifically in all of the integrals). Since 1/b is introduced artifically in the first large integral one may argue that it is permissible to take it out from the end result by replacing it by 1/b1.

At any rate we now adopt the formula

$$B = \frac{1}{b1} \{\}$$

where { } represents the terms in brackets in (15). We now introduce the Lommel-Seeliger law by writing for our final formula

$$B\cos \epsilon = \frac{1}{b^2_1} \{ \} = \frac{\cos^2 i \, \cos^2 \epsilon}{(\cos i + \cos \epsilon)^3} \{ \} .$$

(19)

This is the "new photometric function" used in Chapter II.

Modification of Hapke's Model

We now modify Hapke's model by explicitly truncating the square incident light cylinders at right angles to the incident light. The surface of the cylinder is not the lunar surface. Therefore, the angles i and ϵ do not enter the geometry and the relationship $z \cos i = z' \cos \epsilon$ which basically leads to the Lommel-Seeliger law is no longer applicable. This modification corresponds to case 1(a).

Referring to Figure 4, the total integral is

$$\int_0^{z_0} a(a-x)e^{-z/\tau} dz + \int_0^{z_0} axe^{-(z+z')/\tau} dz'$$

$$+ \, 0 \qquad\qquad + \int_{z_0}^{\infty} a^2 e^{-(z+z')/\tau} dz' \quad .$$

(20)

The first integral is the seen area times the incoming attenuation factor; the second integral is the unseen area times incoming attenuation factor times outgoing attenuation factor. Both integrals are integrated betwen $z = 0$ and $z = z_0$. z_0 is the maximum value for z for which the bottom area can be seen.

$z_0 = a/\tan \alpha$. Both z and z' are measured to the common edge of the seen and unseen area. We will express the integrands in terms of z using the fact that $z' = z/\cos \alpha$. The integrand in the first integral is zero after $z = z_0$ since after that $x = a$. x in the second integral is replaced by a and the integral extended from $z = z_0$ to ∞ as shown in the third integral. In terms of z, (20) becomes

$$= \int_0^{a/\tan\alpha} (a^2 - az\tan\alpha)e^{-z/\tau}dz/\cos\alpha + a\tan\alpha\int_0^{a/\tan\alpha} ze^{-(z+z/\cos\alpha)/\tau}dz/\cos\alpha$$

$$+ a^2\int_{a/\tan\alpha}^{\infty} e^{-(z+z/\cos\alpha)/\tau}dz/\cos\alpha \tag{21}$$

z and z' are measured from the common edge of the seen and the unseen areas.

Carrying out the integrations yields the final result:

$$= \frac{1}{\cos\alpha}\{a^2\tau - a\tau^2\tan\alpha\frac{\cos^2\alpha}{(1+\cos\alpha)^2} + (\frac{a^2\tau}{\tan\alpha} - a^2\tau + a\tau^2\tan\alpha)e^{-a/\tau\tan\alpha} - a\tau^2\tan\alpha$$

$$- \frac{a\tau^2\tan\alpha\cos^2\alpha}{(1+\cos\alpha)^2}e^{-a/\tau(1+1/\cos\alpha)\tan\alpha}\} . \tag{22}$$

The flux of emergent light in terms of the flux of incident light S_0 is then

$$I^{(re)} = \frac{S_o \rho \, b(\alpha)}{\cos \alpha} \left\{ 1 - \frac{\tau}{a} \tan\alpha + \frac{\tau}{a} \frac{\sin\alpha \cos\alpha}{(1+\cos\alpha)^2} + \left(\frac{\tau}{a}\tan\alpha\right) e^{-a/\tau \, \tan\alpha} \right.$$

$$\left. - \frac{\tau}{a} \frac{(\sin\alpha \cos\alpha)}{(1+\cos\alpha)^2} e^{-a(1+\cos\alpha)/\tau \, \sin\alpha} \right\} a^2 \tau \quad . \qquad (23)$$

The appearance of $\cos\alpha$ is the denominator causes the curve for $B(\alpha, g)$ to rise sharply as $\alpha \rightarrow 90°$.

It is interesting to note that if the factor $1/\cos\alpha$ is removed and if we also replace the integrands $e^{-(z+z/\cos\alpha)/\tau}$ by $e^{-2z/\tau}$, that is, discard the $\cos\alpha$ in the integrand also, then the function

$$B(\alpha) = \int_o^{a/\tan\alpha} (a^2 - az\tan\alpha)e^{-z/\tau}\,dz + a\tan\alpha \int_o^{a/\tan\alpha} z e^{-2z/\tau}\,dz + a^2 \int_{a/\tan\alpha}^{\infty} e^{-2z/\tau}\,dz$$

integrates to:

$$B(\alpha) = \frac{a^2 \tau}{2}\left\{ 2 - \frac{3\tau}{2a}\tan\alpha + \frac{2\tau}{a}\tan\alpha \, e^{-a/\tau \, \tan\alpha} - \frac{\tau}{2a}\tan\alpha \, e^{-2a/\tau \, \tan\alpha} \right\} .$$

$$(24)$$

The expression in brackets in (24) is Hapke's retrodirective function $B(\alpha)$.

Neglecting the $1/\cos\alpha$ factor in the preceding derivation is equivalent to attenuation of the light on the way out of the medium (after being scattered) by the same amount as it was attenuated in reaching the scattering center. If the exponentials

are regarded as a measure of probability, then the probability
of penetration to a distance z is taken as the same as a pro-
bability of escaping after being scattered at z. There is no
physical basis for this assumption but it is interesting that by
making it, we arrive at Hapke's retrodirective function. In
the previous derivation of Equation (23), the $1/\cos\alpha$ term
should certainly not be included in the first integral; that is,
the integral involving the light from the seen area which es-
capes back through the incident light tube without attenuation.
With this change, one obtains the following results for
integrations:

The integrals are

$$\int_0^{z_0} a^2 e^{-z/\tau} dz - \int_0^{z_0} a^2 \tan\alpha \, e^{-z/\tau} dz + \int_0^{a/\tan\alpha} z e^{-(z+z/\cos\alpha)/\tau} dz/\cos\alpha$$

$$+ a^2 \int_{a/\tan\alpha}^{\infty} e^{-(z+z/\cos\alpha)} dz/\cos\alpha$$

$$= +a^2\tau - a\tau^2\tan\alpha + \frac{a\tau^2\tan\alpha \, 2\cos\alpha}{(1+2\cos\alpha)^2} + a\tau^2\tan\alpha \, e^{-a/\tau\tan\alpha}$$

$$- \frac{2a\tau^2\tan\alpha\cos\alpha}{(1+2\cos\alpha)^2} e^{-\frac{(1+2\cos\alpha)}{2\tau\sin\alpha}} .$$

We now derive another retrodirective function paying closer
attention to the physical details which should be taken into
consideration in this model. Specifically, we will take into
account the fact that the light scattered from the unseen area

will not attenuate until it escapes from the cylinder. The outgoing attenuation distance must now be measured from the center of the unseen area. This corresponds to case 1(b). This means that before z reaches z_0, $z = 2z'\cos\alpha$. When $z > z_0$, the attenuation path is AP as shown in Figure 5. The integrals then become:

$$\int_0^{a/\tan\alpha} (a^2 - az\tan\alpha)e^{-z/\tau}\,dz + a\tan\alpha\int^{a/\tan\alpha} ze^{-(z+z/2\cos\alpha)/\tau}\,dz/2\cos\alpha$$

$$+ a^2\int_{a/\tan\alpha}^{\infty} e^{-(z+AP)/\tau}\,d(AP) \qquad (25)$$

where upon using the following relations:

$$\ell = \frac{x}{2\tan\alpha}$$

$$\ell' = z - \ell$$

$$AP\cos\alpha = \ell' = z - \frac{a}{2\tan\alpha}$$

$$AP = \frac{\ell'}{\cos\alpha} = \frac{z-\ell}{\cos\alpha} = \frac{z}{\cos\alpha} - \frac{a}{2\tan\alpha\cos\alpha} = \frac{z}{\cos\alpha} - \frac{1}{2\sin\alpha}$$

$$d(AP) = \frac{dz}{\cos\alpha}$$

we obtain the following result for the integrals

$$= \frac{a^2\tau}{2}\left\{ 2 - \frac{2\tau\tan\alpha}{a} + \frac{\tau}{a}\frac{4\sin\alpha}{(1+\cos\alpha)^2} + \left(\frac{2\tau}{a}\tan\alpha\right)e^{-\frac{a}{\tau\tan\alpha}} + \left(-\frac{2}{(1+2\cos\alpha)} - \frac{\tau}{a}\frac{4\sin\alpha}{(1+2\cos\alpha)^2}\right)\right.$$
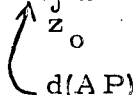
$$\left. \times e^{(1+1/2\cos\alpha)a/\tau\tan\alpha} + \frac{2}{(1+\cos\alpha)}e^{-a/2\tau\sin\alpha}e^{-(1+1/\cos\alpha)/\tau\tan\alpha} \right\} \;.$$

$$(26)$$

Results of the calculations with this expression are discussed in Chapter II.

We now generalize to the extent of allowing the surface facet upon which the incoming light is incident to make an angle β with respect to the normal to the incident light cylinder. However, the incident light attenuation path is measured to center of seen area and attenuation path of light again to and from the unseen area is measured to the center of the unseen area. Again one must average the final result over all values of β. This corresponds to case 2.

Referring to Figure 6 we take CO' as the distance over which the ingoing light hitting the unseen area of the bottom of the cylinder is attenuated. DE is the attenuation distance for the light incident upon the seen area of the bottom of the cylinder. Both distances are parallel to the incident rays and are measured to the midpoint of the unseen and the seen portions respectively of the bottom of the cylinder. Only that portion of the exiting path outside of the cylinder should enter the exponential attenuation factor. The integrals to be evaluated are:

$$\int_{z_{o'}}^{z_o} a(a-x)e^{-DE/\tau}dz + \int_{z_{o'}}^{z_o} axe^{-(O'G+AP)/\tau} + \int_{z_o}^{\infty} a^2 e^{-(z+A'P'')/\tau} d(A'P'') \left\{ \begin{array}{c} \\ d(AP) \end{array} \right. \tag{27}$$

The limit z_o' is introduced since for positive β when α reaches its maximum value of $90°$, z_o is the minimum distance from $z = 0$ at which the area of the scattering center can be seen.

We now write the necessary relationships for case 2. AP is the outgoing attenuation path;

$$CO' = z - \left(\frac{a-x}{2}\right)\tan\beta$$

$$\frac{CO'}{\sin(90+\beta-\alpha)} = \frac{O'P}{\sin(90-\beta)}$$

$$O'P = \frac{\cos\beta}{\cos(\alpha-\beta)}\left[\left(z-\frac{(a-x)}{2}\tan\beta\right)\right]$$

$$AP = O'P - O'A$$

$$O'A = \frac{x}{2\sin\alpha} \quad ; \quad O'A\sin\alpha = \frac{x}{2}$$

$$AP = \frac{z\cos\beta}{\cos(\alpha-\beta)} - \frac{a\cos\beta\tan\beta}{2\cos(\alpha-\beta)} + \frac{x}{2}\frac{\cos\beta\tan\beta}{\cos(\alpha-\beta)} - \frac{x}{2\sin\alpha}$$

$$AP = \frac{z\cos\beta}{\cos(\alpha-\beta)} - \frac{a\sin\beta}{2\cos(\alpha-\beta)} + \frac{x}{2}\left(\frac{\sin\beta}{\cos(\alpha-\beta)} - \frac{1}{\sin\alpha}\right)$$

We now need an expression for x in terms of z.

$$x = BP'\tan\alpha$$

$$BP' = z - \frac{a}{2}\tan\beta$$

$$x = z\tan\alpha - \frac{a}{2}\tan\alpha\tan\beta$$

Thus

$$x = c\,z + d$$

where

$$c = \tan\alpha \text{ and } d = -\frac{a\tan\alpha\tan\beta}{2}$$

$$AP = \frac{z\cos\beta}{\cos(\alpha-\beta)} - \frac{a}{2}\frac{\sin\beta}{\cos(\alpha-\beta)} + \frac{z\tan\alpha}{2}\left(\frac{\sin\beta}{\cos(\alpha-\beta)} - \frac{1}{\sin\alpha}\right)$$

$$- \frac{a}{4}\tan\alpha\tan\beta\left(\frac{\sin\beta}{\cos(\alpha-\beta)} - \frac{1}{\sin\alpha}\right)$$

$$= z\left(\frac{\cos\beta}{\cos(\alpha-\beta)} + \frac{\tan\alpha\tan\beta\cos\beta}{2\cos(\alpha-\beta)} - \frac{\tan\alpha}{2\sin\alpha}\right)$$

$$- \frac{a}{2}\frac{\cos\beta}{\cos(\alpha-\beta)}\tan\beta - \frac{a}{4}\frac{\tan\alpha\tan^2\beta\cos\beta}{\cos(\alpha-\beta)} + \frac{a}{4}\frac{\tan\alpha\tan\beta}{\sin\alpha}$$

or AP = Az+B, where

$$A = \frac{\cos\beta}{\cos(\alpha-\beta)}\left(1 + \frac{\tan\alpha \tan\beta}{2}\right) - \frac{1}{2\cos\alpha}$$

and

$$B = -\frac{a}{2}\frac{\cos\beta\tan\beta}{\cos(\alpha-\beta)}\left(1 + \frac{\tan\alpha\tan\beta}{2}\right) + \frac{a}{2}\frac{\tan\beta}{\cos\alpha} \; .$$

In the second integral $dz' = d(AP) = Adz$. In the first integral we shall take $dz' = dz$. When $x = a$, $z = z_o$, the maximum z for which the bottom can be seen at a given α.

We now obtain an expression for $A'P''$ in terms of z. For example $cP'E$:

$$\frac{z_o + \frac{a\tan\beta}{2}}{\sin(90+\beta-\alpha)} = \frac{a/\cos\beta}{\sin\alpha}$$

$$z_o = \frac{a\cos(\alpha-\beta)}{\sin\alpha\cos\beta} - \frac{a}{2}\tan\beta$$

After $z = z_o$ the following relations hold:

$$A'B' = \frac{a}{2}\cot\alpha \qquad L'A' = \frac{a}{2\sin\alpha}$$

$$\frac{A'P''}{A'P''+L'A'} = \frac{z - \frac{a}{2}\tan\beta - \frac{a}{2}\cot\alpha}{z}$$

$$\frac{A'P''}{A'P''+L'A'} = \frac{z-\ell}{z}$$

where

$$\ell = \frac{a}{2}(\tan\beta + \cot\alpha)$$

$$A'P'' = \frac{z\ L'A' - \ell L'A'}{\ell}$$

$$A'P'' = z\frac{a}{2\ell\sin\alpha} - \frac{a}{2\sin\alpha} = \frac{a}{2\sin\alpha}\left(\frac{z}{\ell} - 1\right)$$

$$= c_2 z + d_2$$

where

$$c_2 = \frac{a}{2\ell\sin\alpha} = \frac{1}{\sin\alpha(\tan\beta + \cot\alpha)} \ ; \ d_2 = -\frac{a}{2\sin\alpha}$$

$$dz' = d(A'P'') = \frac{a}{2\ell\sin\alpha}\ dz$$

Incoming attenuation distance for area which can be seen is

$$DE = z + \frac{x}{2}\tan\beta = z + \frac{z}{2}\tan\beta\tan\alpha - \frac{a}{4}\tan\alpha\tan^2\beta$$

$$= z\left(1 + \frac{\tan\alpha\tan\beta}{2}\right) - \frac{a}{4}\tan\alpha\tan^2\beta$$

$$DE = c_1 z + d_1$$

where

$$c_1 = 1 + \frac{\tan\alpha \ \tan\beta}{2}$$

$$d_1 = -\frac{a\tan\alpha \ \tan^2\beta}{4}$$

Incoming attenuation distance for area which cannot be seen is

$$CO' = z - \left(\frac{a-x}{2}\right)\tan\alpha = z + \frac{x}{2}\tan\alpha - \frac{a}{2}$$

$$= z + \frac{z}{2}\tan^2\alpha - \frac{a}{4}\tan^2\alpha \ \tan\beta - \frac{a}{2}$$

$$CO' = z\left(1 + \frac{\tan^2\alpha}{2}\right) - \frac{a}{2}\left(1 + \frac{\tan^2\alpha \ \tan\beta}{2}\right)$$

$$= c_3 \ z + d_3$$

where

$$c_3 = 1 + \frac{\tan^2\alpha}{2}$$

$$d_3 = -\frac{a}{2}\left(1 + \frac{\tan^2\alpha \ \tan\beta}{2}\right)$$

Integrals (20) are explicitly for this case:

$$\int_0^{z_0} (a^2 - acz - ad) e^{-(c_1 z + d_1)/\tau} dz + \int_0^{z_0} a(cz+d) e^{-[(c_3 z + d_3) - (Az+B)]/\tau} A dz$$

$$+ \int_{z_0}^{\infty} a^2 e^{-(z + c_2 z + d_2)/\tau} c_2 dz$$

where: a^2 = area of intercepting element

$c = \tan\alpha$

$d = \dfrac{-a \tan\alpha \tan\beta}{2}$

$A = \dfrac{\cos\beta}{\cos(\alpha - \beta)} \left(1 + \dfrac{\tan\alpha \tan\beta}{2}\right) - \dfrac{1}{2\cos\alpha}$

$B = -\dfrac{a}{2} \dfrac{\cos\beta \tan\beta}{\cos(\alpha - \beta)} \left(1 + \dfrac{\tan\alpha \tan\beta}{2}\right) + \dfrac{a}{2} \dfrac{\tan\beta}{\cos\alpha}$

$z_0 = \dfrac{a \cos(\alpha - \beta)}{\sin\alpha \cos\beta} - \dfrac{a}{2} \tan\beta$

Evaluation of integrals;

$$(a^2 - ad) e^{-d_1/\tau} \int_0^{z_0} e^{-c_1 z/\tau} dz - ace^{-d_1/\tau} \int_0^{z_0} z e^{-c_1 z/\tau} dz$$

$$+ adA e^{-(d_3 + B)/\tau} \int_0^{z_0} e^{-(c_3 + A)z/\tau} dz + acA e^{-(d_3 + B)/\tau} \int_0^{z_0} z e^{-(c_3 + A)z/\tau} dz$$

$$+ a^2 e^{c_2 - d_2/\tau} \int_{z_0}^{\infty} e^{-(1 + c_2)z/\tau} dz \qquad\qquad (28)$$

where:

$$d = - \frac{\tan\alpha \tan\beta}{2}$$

$$c_1 = 1 + \frac{\tan\alpha \tan\beta}{2}$$

$$c = \tan\alpha$$

$$d_1 = - \frac{\tan\alpha \tan^2\beta}{4}$$

$$A = \frac{\cos\beta}{\cos(\alpha-\beta)} \left(1 + \frac{\tan\alpha \tan\beta}{2}\right) - \frac{1}{2\cos\alpha}$$

$$c_3 = 1 + \frac{\tan^2\alpha}{2}$$

$$d_3 = - \frac{1}{2}\left(1 + \frac{\tan^2\alpha \tan\beta}{2}\right)$$

$$B = - \frac{1}{2} \tan\beta\, A$$

$$c_2 = \frac{1}{\sin\alpha\,(\tan\beta + \cot\alpha)}$$

$$d_2 = - \frac{1}{2\sin\alpha}$$

$$z_o = \frac{\cos(\alpha-\beta)}{\sin\alpha\cos\beta} - \frac{1}{2}\tan\beta$$

$$z_o' = \frac{a}{2}\tan\beta$$

The final result of integrating gives:

$$B(\alpha, \beta, g) = a^2 \tau \left\{ \left[-\left\{ \frac{1-d}{c} - g \frac{c}{c_1^2} \right\} + \frac{c z_o}{c_1} \right] e^{-d_1 g} e^{-c_1 z_o g} \right.$$

$$+ \left[-\left\{ \frac{dA}{c_3+A} + g \frac{c}{(c_3+A)^2} \right\} - \frac{cA z_o}{c_3+A} \right] e^{-(d_3+B)g} e^{-(c_3+A)g}$$

$$- \left[-\left\{ \frac{1-d}{c_1} - g \frac{c}{c_1^2} \right\} + \frac{c z_o}{c_1} \right] e^{-d_1 g} e^{-c_1 z_o' g}$$

$$- \left[-\left\{ \frac{dA}{c_3+A} + g \frac{c}{(c_3+A)^2} \right\} - \frac{cA z_o'}{c_3+A} \right] e^{-(d_3+B)g} e^{-(c_3+A)z_o g}$$

$$\left. + \frac{c^2}{1+c_2} e^{-d_2 g} e^{-(1+c_2)z_o g} \right\} \qquad (29)$$

The preceeding retrodirective function must now be multiplied by the probability that a slope will have a given value. If there is any significance to a distribution of slopes the distribution must be about the local normal to the mean lunar surface (or defined with respect to a tangent to the mean linear surface). For the purposes of atrial calculation we shall take a very simple weight function, for example the probability of a given slope may be the same between $+60°$ and $-60°$ measured from the tangent to the mean lunar surface. Let β' be the angle between the surface facet and the mean lunar surface. See Figure 7 . The retrodirective function has been derived in terms of the angle β which is the angle between the surface facet and normal to the direction of the incident light. Therefore it is necessary to relate β' to β. One should note that

if the retrodirective function is integrated over a range of slopes then the Lommel-Seeliger factor should be modified to take into account the fact that the lunar surface is made up of many facets and modify the derivation of the Lommel-Seeliger law accordingly. This will be done shortly. In the mean time we denote the modified Lommel-Seeliger factor by $L(i,\epsilon,\alpha,\beta)$ where it is now a function of α and β as well as i and ϵ. The scattering function will be denoted by $s(\alpha)$. Thus the integral to be performed is

$$\int L(i,\epsilon,\alpha,\beta)S(\alpha)B(\alpha,g,\beta)f(\beta')d\beta'$$

divided by a normalizing factor $\int f(\beta')d\beta'$. In general $d\beta'=d\beta$. The general integral can be expressed in terms of β and is therefore of the form:

$$L(i,\epsilon,\alpha,\beta)B(\alpha,g,\beta)d\beta \qquad\qquad (30)$$

We have now introduced the fact that $f(\beta') = f(\beta) = 1$, One must now simply be careful in stating the limits when the integration in β is carried out. The limits will be affected by the value of the angle of incidence, i, with respect to the normal of the mean lunar surface. For computer evaluation of the integral one will specify a value of τ/a and also a value of α. We must now also specify the value of i. For each set of these three quantities one will carry out an

integration over β . In order to illustrate the limits on β we give a specific example.

    1. Say $\beta'_{max} = \beta'_m = 60°$. If $i = 35°$ β will range from 0 to 6-35 = $|\beta'_m|$ -i. For positive β , α range is $0°$ to line of horizon (mean lunar surface), that is, to 90-i. Thus for any $\alpha,0°$ to $90°$-i, integrate β from $0°$ to $|\beta'_m|$-i. See Figure 9b.

        a. For negative β , $\beta < i$; for α's less than 90-(i-β') integrate β from 0 to -i. Figure 9(c).

        b. For negative β , $|\beta| > i$; for α's less than 90-(i-β') integrate β from 0 to -i-β_{max} or only to $-90°$ if $|i+\beta_{max}| > 90°$. Figure 9(d).

The above routine must be carried out for each value of α for various values of i.

Modification of Lommel-Seeliger Factor

If one makes a correction to the retrodirective function associated with the inclination of the lunar facets, then the Lommel-Seeliger law should be modified in a similar way in order to consistently treat all factors in the overall brightness. Referring to Figure 8, AM represents the mean lunar surface and MP a surface facet. OO' is the direction of incident light and O'P the direction of outgoing light. AO' = y is the perpendicular distance of O' below the mean lunar surface. The outgoing light will be attenuated over the distance O'P rather than the distance O'M as in the usual Lommel-Seeliger derivation. In the present derivation we consider the special case where angles i, ϵ and α are all in the same plane. We will then average the modified Lommel-Seeliger law so derived by weighting the resulting function by the factor $f(\beta)$. Although this procedure is not general it should give one a good measure of the importance of recognizing the distribution of slopes over the lunar surface. From triangle OPM, by law of sines:

$$\frac{OP}{\sin(90-i-\alpha)} = \frac{PM}{\sin \beta}$$

$$PM = \frac{OP \sin \beta}{\sin(90-i-\alpha)}$$

From triangle OO'P:

$$\frac{OP}{\sin \alpha} = \frac{z'}{\sin(90+i-\beta)}$$

Thus

$$PM = \frac{z'\sin\beta\sin\alpha}{\sin(90-i-\alpha)\sin(90+i-\beta)}$$

$$= \frac{z'\sin\beta\sin\alpha}{\cos(i+\alpha)\cos(i-\beta)}$$

Thus the usual relationship

$$y = z\cos i = z'\cos\epsilon$$

used in deriving the Lommel-Seeliger law is replaced by

$$y = z\cos i = (z'+PM)\cos\epsilon$$

Thus

$$y = z\cos i = z'\cos\epsilon \left(1+ \frac{\sin\beta\sin\alpha}{\cos(i+\alpha)\cos(i-\beta)}\right).$$

Equation 4-21 would then be replaced by

$$LS = f_o E_o \frac{1}{\dfrac{1}{\cos i} + \dfrac{1}{\cos\epsilon}\left(1+\dfrac{\sin\beta\sin\alpha}{\cos(i+\alpha)\cos(i-\beta)}\right)}$$

This expression is not symmetrical in i and ϵ. To symmetrize it we multiply cosi by the same correction factor but replace i by ϵ in the correction factor. Thus the Lommel-Seeliger law

which we will work with will be the following:

$$LS = \frac{f'_o E_o}{\cfrac{1}{\cos i\left(1+\cfrac{\sin\beta\sin\alpha}{\cos(\epsilon+\alpha)\cos(\epsilon-\beta)}\right)} + \cfrac{1}{\cos\epsilon\left(1+\cfrac{\sin\beta\sin\alpha}{\cos(i+\alpha)\cos(i-\beta)}\right)}}$$

(31)

Since $\alpha = \epsilon - i$, this can also be written, after changing

$$1+\frac{\sin\beta\sin\alpha}{\cos(i+\alpha)\cos(i-\beta)} \qquad \text{to} \qquad 1+\frac{\sin\beta\sin(\epsilon-i)}{\cos\epsilon\cos(i-\beta)}$$

and then cosi by the same terms after interchanging i and ϵ.

$$LS = \frac{f_o E_o}{\cfrac{1}{\cos i\left(1+\cfrac{\sin\beta\sin(i-\epsilon)}{\cos i\cos(\epsilon-\beta)}\right)} + \cfrac{1}{\cos\epsilon\left(1+\cfrac{\sin\beta\sin(\epsilon-i)}{\cos\epsilon\cos(i-\beta)}\right)}}$$

(32)

Note that in Equation (32) when the correction term to $\cos\epsilon$ is positive the correction term to cosi is negative. Therefore symmetrization may over compensate introducing too large a correction to cosi. It may therefore be more reasonable physically to divide each correction term by 2 so that a better approximate formula may be:

$$LS = \cfrac{f_o E_o}{\cfrac{1}{\cos i\left(1+\cfrac{\sin\beta\sin(i-\epsilon)}{2\cos i\cos(\epsilon-\beta)}\right)} + \cfrac{1}{\cos\epsilon\left(1+\cfrac{\sin\beta\sin(\epsilon-i)}{2\cos\epsilon\cos(i-\beta)}\right)}}$$

$$(33)$$

In terms of α and i this equation becomes

$$LS = \cfrac{f_o E_o}{\cfrac{1}{\cos i\left(1-\cfrac{\sin\beta\sin\alpha}{2\cos i\cos(\alpha+i-\beta)}\right)} + \cfrac{1}{\cos(\alpha+i)\left(1+\cfrac{\sin\beta\sin\alpha}{2\cos(\alpha+i)\cos(i-\beta)}\right)}}$$

$$(34)$$

For the special case $i = 0$

$$LS = \cfrac{f_o E_o}{\cfrac{1}{1-\cfrac{\sin\beta\sin\epsilon}{2\cos(\epsilon-\beta)}} + \cfrac{1}{\cos\epsilon\left(1+\cfrac{\sin\beta\sin\epsilon}{\cos\epsilon\cos\beta}\right)}} \qquad (35)$$

In this case $\alpha = \epsilon$ so α can replace ϵ for computation purposes.

Numerical Calculations

For cases 1(a) and 1(b) the total light flux i reaching a detector of area a is given by the product of three factors. (1) The Lommel-Seeliger factor: $\frac{1}{1+\cos\epsilon/\cos i}$. In this form the fact that one is looking at a projected area has been taken into account since the energy out per unit area of surface given by Equation 4-21 has been divided by $\cos\epsilon$. (2) The scattering function $b(\alpha)$. (3) The retrodirective function $B(\alpha,g)$. For the retrodirective function one may use any of the expressions previously derived. The product of these factors must be multiplied by $S_0\rho Ad\Omega$. S_0 is solar energy per unit area of solar beam. The fact that this is spread over a lunar area $1/\cos i$ was taken into account in deriving the Lommel-Seeliger factor. $d\Omega$ is the solid angle subtended at the surface of the detector: $d\Omega = a/R^2$ where a is the area of the detector. $Ad\Omega = \frac{Aa}{R^2} = ad\omega$ where $d\omega$ is the angle subtended by the viewed lunar area. $d\omega$ will be governed by the length of the detector tube (See Figure 9). ρ is the coefficient of reflection of the lunar matter. The final expression is then

$$i = S_0 a\rho\, b(\alpha)\frac{B(\alpha,g)}{1+\cos\epsilon/\cos i}d\omega \ . \qquad (36)$$

In applying Equation (36) to the moon as observed from the earth, we shall proceed as if the intensity equator coincides with the geographic equator and that the subearth point falls on this line at the center of the lunar coordinate system. Then if $\hat{n}$ is the unit normal at the area of interest on the lunar surface, β the

lunar latitude of the area, λ its longitude, and φ the lunar phase angle, one can write (see Figure 10):

$$\hat{n} = \sin\beta\,\hat{k} + \hat{j}\cos\beta\,(\varphi+\lambda) + \hat{i}\cos\beta\,\sin(\varphi+\lambda)$$

$$\vec{I} = \vec{j}$$

$$\cos i = \hat{n}\cdot\vec{I} = \cos\beta\cos(\varphi+\lambda)$$

$$\vec{E} = \hat{j}\cos\varphi + \hat{i}\,\sin\varphi + \hat{k}\cdot 0$$

$$\hat{n}\cdot\vec{E} = \cos\varphi\,\cos\beta\cos(\varphi+\lambda) + \sin\varphi\cos\beta\sin(\varphi+\lambda)$$

$$= \cos\beta[\cos\varphi\cos(\varphi+\lambda) + \sin\varphi\sin(\varphi+\lambda)]$$

$$\cos\epsilon = \hat{n}\cdot\vec{E} = \cos\beta\,\cos\lambda$$

$$\alpha = |\varphi|.$$

Making these substitutions in Equation (36), the light reflected into a terrestrial detector from a small region of the surface at position (λ,β) on the moon, at phase angle φ is

$$i(\varphi,\lambda,\beta) = S_o\,ad\omega\,\frac{\sin|\varphi| + (\pi - |\varphi|)\cos|\varphi|}{\pi}\,\frac{1}{1+\cos\lambda/\cos(\lambda+\varphi)}\,B(\alpha,g).$$

$$(37)$$

In the formula we have used the backscattering function

$$b(\alpha) = (\sin\alpha + (\pi-\alpha)\cos\alpha/\pi.$$

Note that when $\lambda + \varphi = 90°$, the Lommel-Seeliger factor requires $i(\varphi,\lambda,\beta)$ to be zero.

REFERENCES FOR CHAPTER III

1. J. van Diggelen, "Photometric Properties of Lunar Carter Floors," <u>Recherces Astronomiques de l'Observatoire d'Utrecht</u> <u>14</u>, No. 2 (1960).

2. V. A. Fedoretz, Utch. Zap. Kharhov Univ., <u>42</u>, 49 (1952).

3. B. W. Hapke, Journal of Geophysical Research <u>68</u>, 4571 (1963).

4. G. Rougier, <u>Ann. de l'Observatoire de Strassbourg</u> <u>2</u>, 319 (1933).

5. H. C. Van deHulst, "The Atmospheres of the Earth and Planets," U. of Chicago Press (1948).
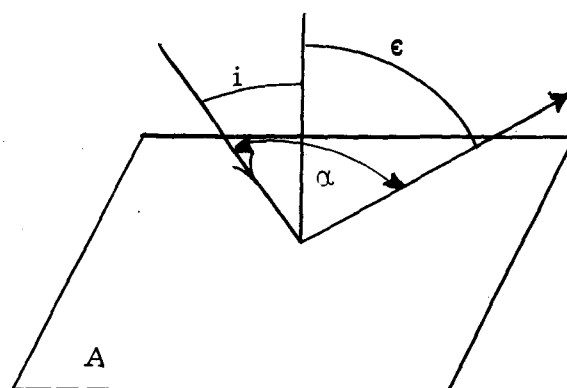
Figure 1.   Reflecting area A showing angle of incidence i,
angle of reflection ϵ, angle α.
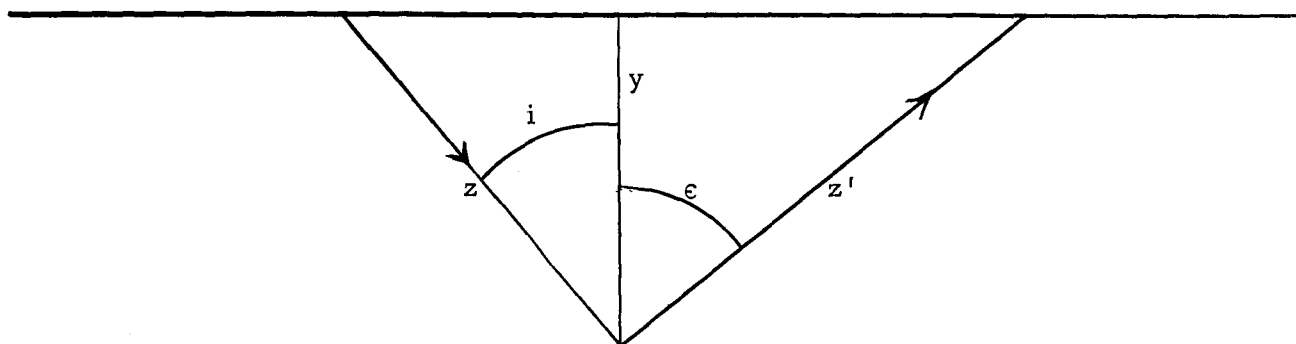
Figure 2.   Incoming path z and outgoing z' after scattering of
light from a point vertical distance y in medium.
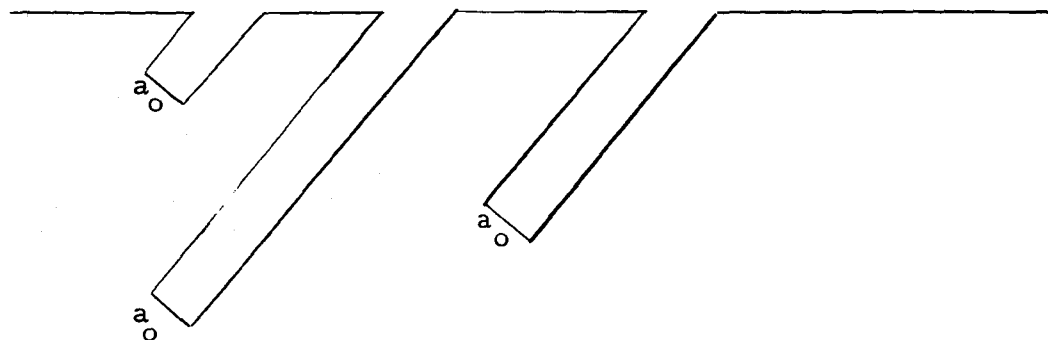
Figure 3.   Scattering area a_o and corresponding empty light tubes.
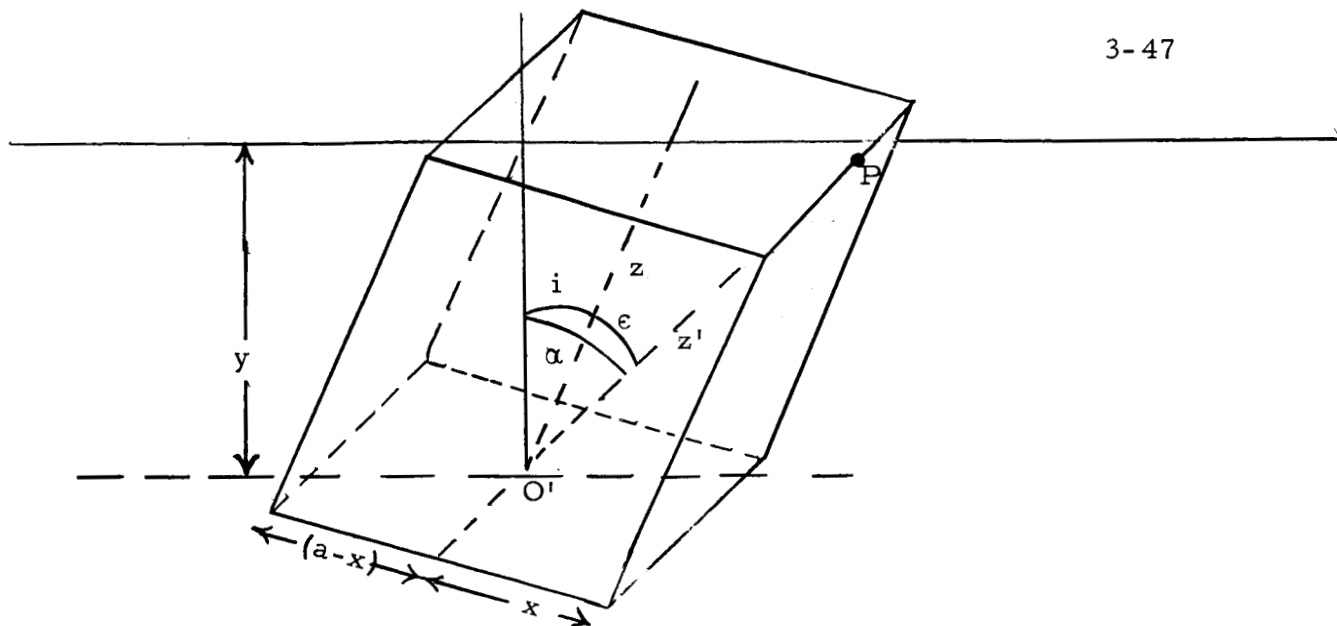
Figure 4.   Figure used for deriving Hapke's photometric function.
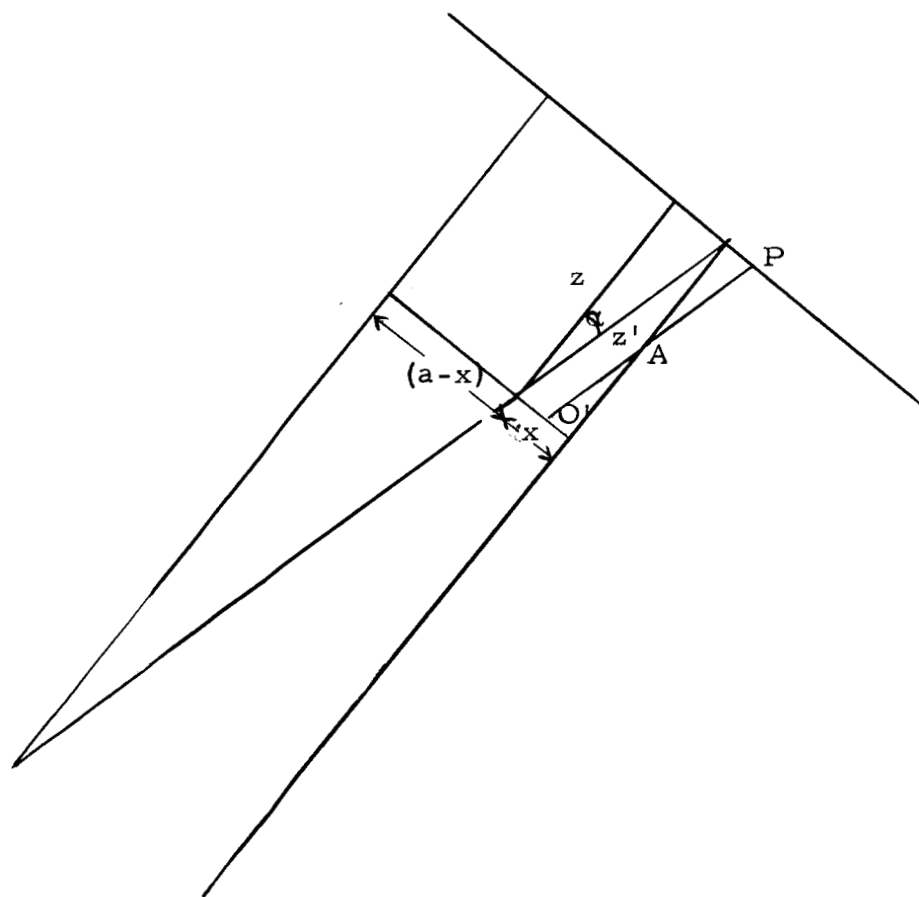
Figure 5.   Figure for deriving modified retrodirective function.

Figure 6. Figure for deriving modified retrodirective function when facet makes angle β with mean lunar surface.
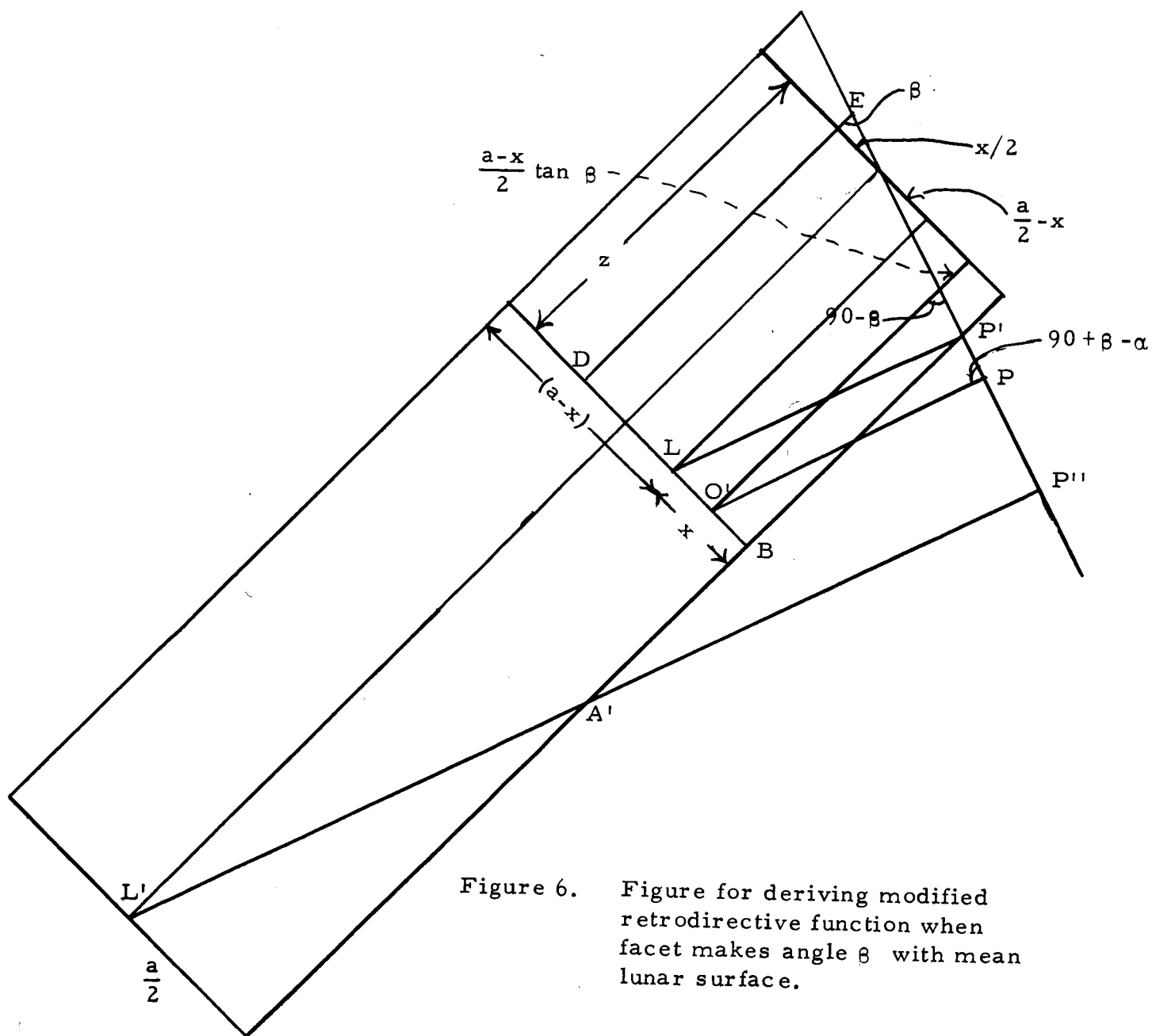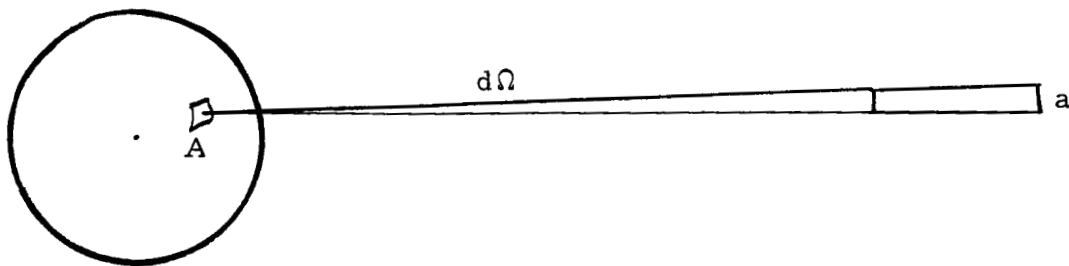
Figure 7.   Collimator tube, detector a and viewed area A on the lunar surface.
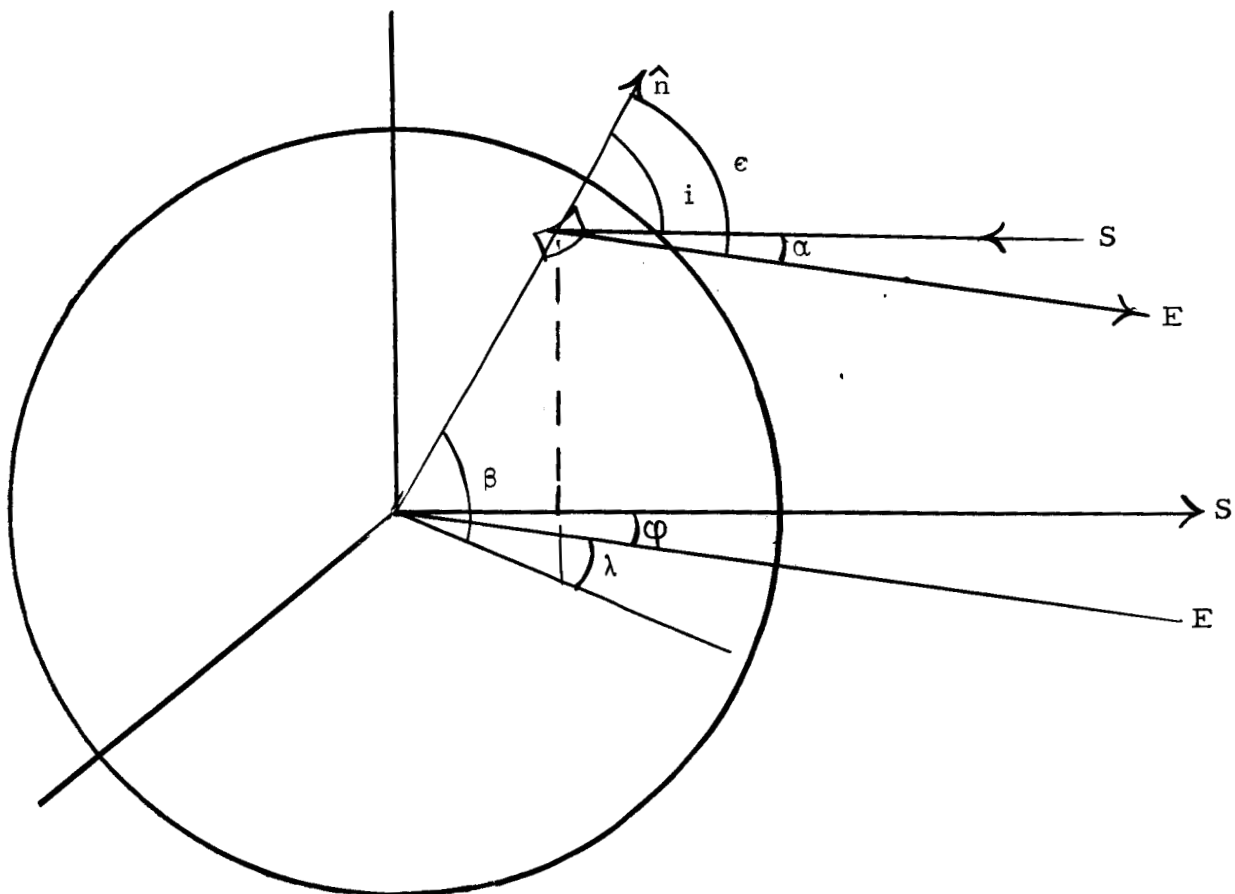
Figure 8.   Relationship between ε, i, α, and lunar latitude ß, longitude λ, and lunar phase angle φ .

(a)

(b)

(c)

Fig. 9

(d)
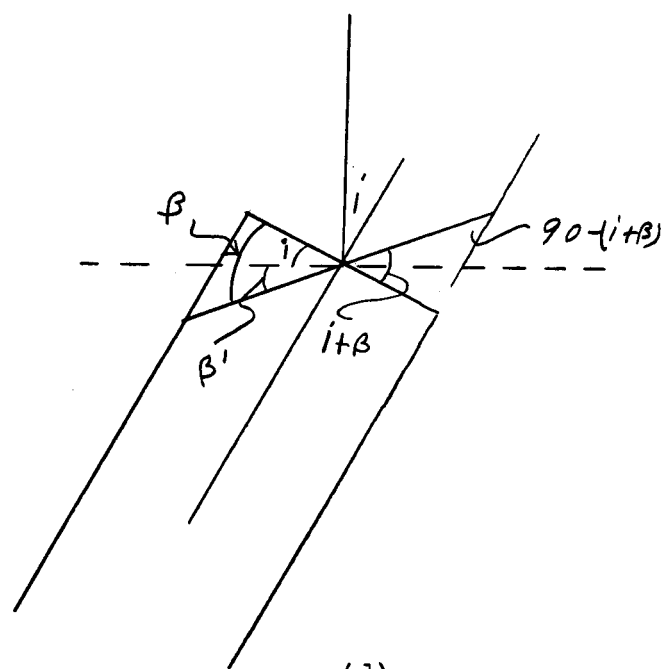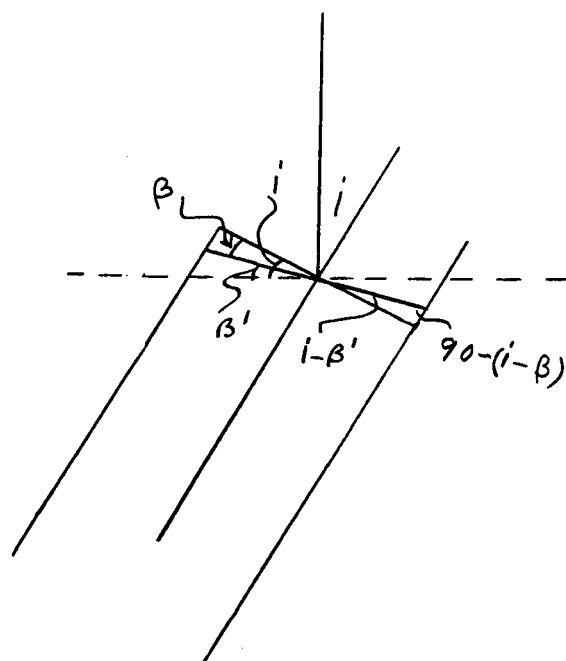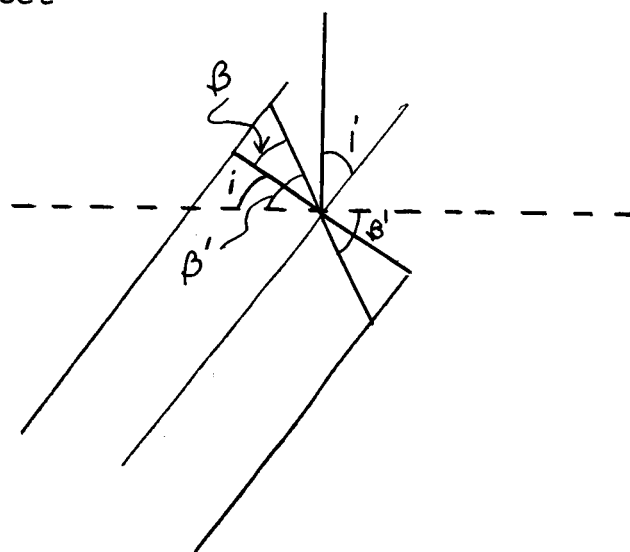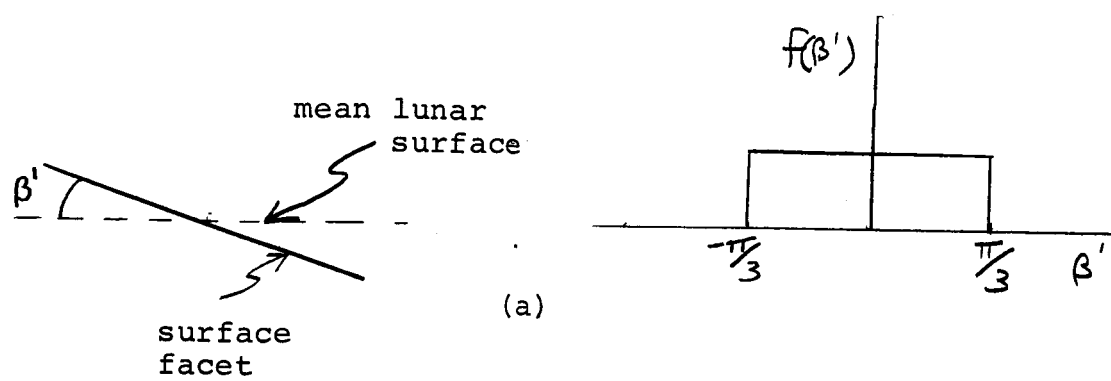
CHAPTER IV

MATHEMATICAL EXPRESSION FOR INFRARED RADIATION
FROM THE LUNAR SURFACE

Introduction

In this chapter we shall give a heuristic argument leading
to a mathematical expression for the infrared radiation emitted
from the lunar surface. A number of comparisons with experimental
data of Pettit and Nicholson,[1] Sinton,[2] and Saari and Shorthill,[3]
will be made. Tables of the calculated emitted energy are
given in the Appendix for angles of incidence 80°, 60°, 30°,
and 0°, for angles of observation every 5° from 0° to 85°, and
for azimuthal angles between incident and observed rays every
15° from 0° to 180°.

In this work we do not consider wavelength dependence of
the energy; only the total energy integrated over all wavelengths
is considered. We also neglect slight differences in albedo of
the different lunar formations. Such differences between maria
and terrae, for example, will lead to the terrae's being slightly
cooler by perhaps a degree Kelvin or so, under the same conditions
of illumination, than the maria. These differences are smaller
than the accuracy of the mathematical expression to be presented.

We shall also neglect differences in temperature between
morning and evening, although the data of Saari and Shorthill
seem to indicate that, at a given angle of incidence and angle of
observation the morning brightness temperature is slightly
warmer than the evening brightness temperature.

Under these assumptions the angular distribution of emitted radiation is a function only of the geometry of the incident and observed rays with respect to the normal to the lunar surface at the position of the point being observed (see Figure 3).

Heuristic Derivation of Expression for Emitted Energy

Consider a vertical cliff of height h, with the line of the cliff c, at right angles to the sun's rays which illuminate the surface at angle of incidence i, as in Figure 1. The bottom of the cliff is at B, the edge of the shadow is at S, a distance BS = htani from the cliff. Suppose this shadow is observed from the angle of observation ϵ, with the phase angle given by

$$\alpha = i + \epsilon \quad . \tag{1}$$

Dropping perpendicular from B to the rays AE, DE' which delimit the region of shadow as observed from the earth, we see that

$$AB = h\sin\epsilon$$

$$BD = h\tan i\cos\epsilon$$

So
$$AB + BD = h(\tan i \cos\epsilon + \sin\epsilon)$$

$$= \frac{h}{\cos i}(\sin i \cos\epsilon + \sin\epsilon \cos i) = \frac{h\sin\alpha}{\cos i} \quad .$$

$$\tag{2}$$

Thus a cliff of height h, when illuminated at angle of incidence i and observed at angle ϵ such that $i + \epsilon = \alpha$, will give rise to an area of shadow as projected in the direction of observation, of $h\sin\alpha/\cos i$.

Consider the situation of Figure 2, in which the phase angle is given by $\alpha = i - \epsilon$. Now the shadowed face of the cliff is not visible. Dropping a perpendicular from S to A, the direction of observation of C extended, we wish to calculate the distance SA. From the figure we have

$$BS = h\tan i$$

$$BD = h\tan \epsilon$$

$$AF = BD\cos \epsilon = h\sin \epsilon$$

$$SA = BS\cos \epsilon - AF = h\tan i \cos \epsilon - h\sin \epsilon$$

$$= h\sin\alpha/\cos i \qquad (3)$$

which is the same result as before. In Figure 2 if $\epsilon > i$ no shadow is seen; in fact some of the illuminated area is obscured by the top of the cliff. Therefore the expression $h\sin\alpha/\cos i$ for the projected shadow area is not always a correct expression. Further pursuit of the correct expression for a particular model results in a variety of complicated trigonometrical formulae which are not particularly enlightening. Let us take the result $h\sin\alpha/\cos i$ literally and see what it implies.
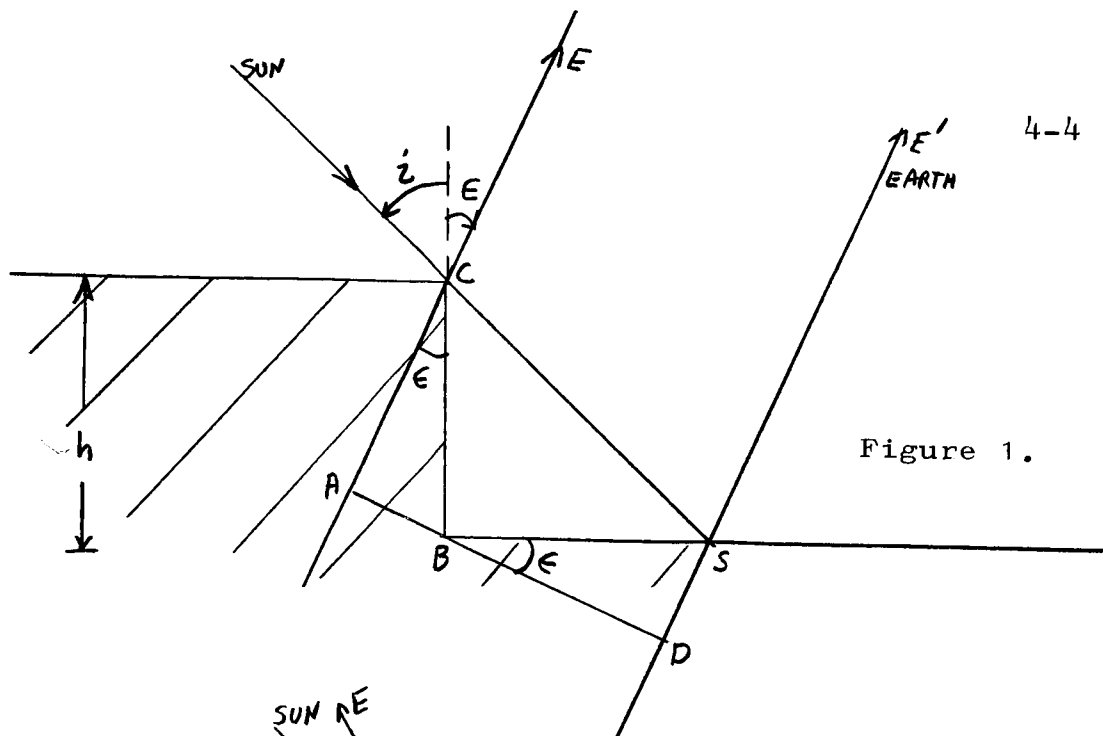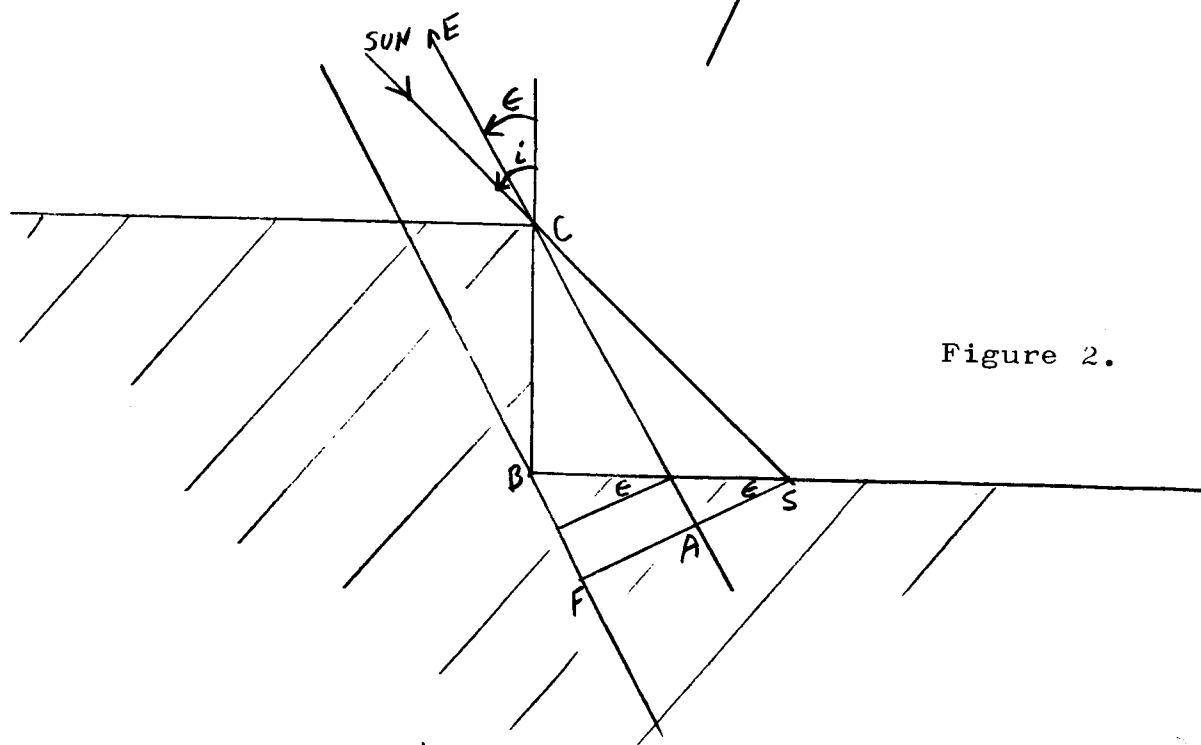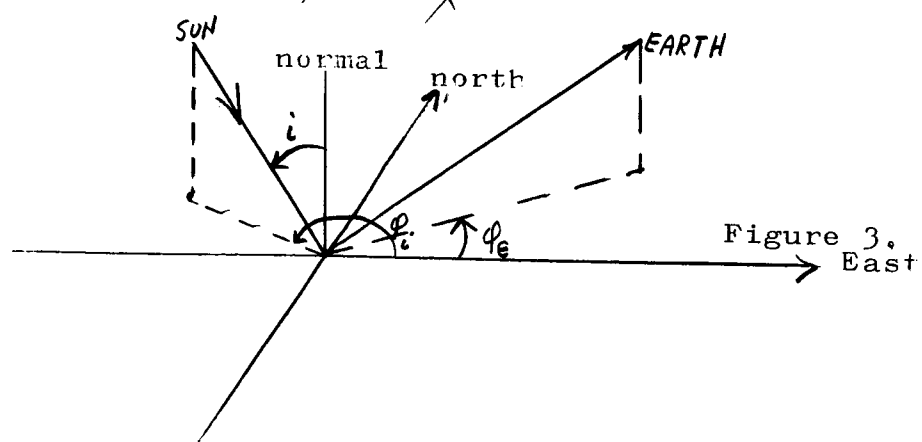
Figure 1.

Figure 2.

Figure 3.

Suppose that there were a large number of such cliffs on the lunar surface, with some characteristic distance between them. The flat surface between cliffs, which is illuminated at angle of incidence i and observed at phase angle α, we assume emits in accordance with some law $E(i, \epsilon, \alpha)$ (in $cal/cm^2 min$). Some of the projected area is in shadow, and is therefore not emitting. The larger the shadowed area is, the smaller will be the amount of energy received by the detector. It seems reasonable to assume that the fraction of shadowed area increases as $\sin\alpha / \cos i$, so that the energy emitted in the direction of the detector will be

$$\frac{E(i, \epsilon, \alpha)}{1 + a_4 \frac{\sin\alpha}{\cos i}} \tag{4}$$

where a_4 is some parameter determined by the relationship between cliff heights and distances between cliffs. The above expression has some reasonable characteristics: At large angles of incidence, where the shadows are exceptionally long, the term $a_4 \sin\alpha / \cos i$ becomes very large and the emitted energy becomes small. Also at zero phase angle, $\alpha = 0$, the correction in the denominator is zero, so that no shadows would be observed. These are certainly features that would have to be preserved in a more exact treatment of the model. The features give the energy some strong directional characteristics.

The law $E(i, \epsilon, \alpha)$ may also have some directional features. If the illuminated portion of the surface emits like a black

body, $E(i, \epsilon, \alpha)$ will be proportional to the energy available per unit area, $S_o \cos i$, where S_o is the solar constant. Our studies of the lunar infrared radiation at the subsolar point indicate that $E(i, \epsilon, \alpha)$ must also have some directional component which has the following characteristics

(a) The directional component is peaked at $\alpha = 0$.

(b) It is zero when $\epsilon = \pi/2$.

(c) It varies trigonometrically rather than exponentially or algebraically; at the subsolar point it behaves as $\cos \epsilon$ or $\cos \alpha$.

These features indicate that $E(i, \epsilon, \alpha)$ might be of the form

$$E(i, \epsilon, \alpha) = a_1 \cos i + a_2 \cos \alpha . \qquad (5)$$

However this does not agree with experiments too well at large angles of incidence or observation, approaching 90°. Further, it does not satisfy condition (2), above.

This expression has most of the features necessary for a good fit with experiment except the directional component $a_2 \cos \alpha$ does not vanish at $\epsilon = \pi/2$ as it should (except when i =0).

We therefore assume that some more exact model calculation would give rise to such a function, due perhaps to directional radiation from crater bottoms, which vanishes at $\epsilon = \pi/2$. We have tried to invent such functions; the simplest one is obtained by replacing $\cos \alpha$ by $\cos \alpha'$ where

$$\alpha' = \alpha'(i,\epsilon) = \frac{\pi}{2}\sqrt{\frac{i^2+\epsilon^2-2i\epsilon\cos(\varphi_i-\varphi_\epsilon)}{\frac{\pi^2}{4}+\frac{4}{\pi^2}i^2\epsilon^2-2i\epsilon\cos(\varphi_i-\varphi_\epsilon)}}$$

$$(6)$$

where $\varphi_i, \varphi_\epsilon$ are the azimuthal angles of the incident and observed rays, respectively, measured with respect to some fixed direction such as the easterly direction on the lunar surface (see Figure 3).

We did not derive this expression, we simply invented it; there are obviously an infinite number of such functions of which this is only the simplest. One can easily verify that $\cos\alpha'$ has the three characteristics listed above Equation (5).

(a) At $\alpha=0$, $i=\epsilon$ and $\varphi_i=\varphi_\epsilon$ so $\alpha'=0$ and $\cos\alpha'=1$, so the peak occurs at $\alpha=0$ and nowhere else.

(b) When $\epsilon=\pi/2$, $\alpha'=\pi/2$ so $\cos\alpha'=0$; the function thus vanishes at these limits.

(c) The variation of $\cos\alpha'$ between these extremes is smooth and trigonometrical in nature.

Further study indicates that there is an additional directional component which is not affected by shadowing of the type which gives rise to the expression (7). If there are rocks littering the flat surface, which are more or less spherical in shape and each part of the surface of which emits like a black body, then such a spherical body would give rise to an emitted energy proportional to

$$\frac{1}{\pi}\{ (\pi - |\alpha|)\cos|\alpha| + \sin|\alpha| \} \tag{7}$$

where $|\alpha|$ is the magnitude of the phase angle. This Shoenberg function arises from integration of the emitted energy from an illuminated black body and takes account of the fact that the shadowed portion of the sphere does not emit. We may think of a contribution like this as being due to either rocks littering the highlands or to high domes and peaks which shadow themselves to a certain extent.

With this addition, the emitted energy is written in the form per unit solid angle

$$I^{em}(i,\epsilon,\alpha) = B(i,\epsilon,\alpha)\cos\epsilon \tag{8}$$

where $B(i,\epsilon,\alpha)$ is the radiance and $\cos\epsilon$ is a geometrical factor. I^{em} and B will have physical dimensions of calories/cm^{2}min per sterad. $B(i,\epsilon,\alpha)$ will be of the form

$$B(i,\epsilon,\alpha) = \frac{a_1\cos i + a_2\cos\alpha'}{1 + a_4\frac{\sin\alpha}{\cos i}} + a_3\frac{1}{3\pi}\{ (\pi - |\alpha|)\cos|\alpha| + \sin|\alpha| \}, \tag{9}$$

where a_1, a_2, a_3 and a_4 are adjustable parameters.

To avoid difficulties which arise with the expression $\sin\alpha/\cos i$ at large phase angles, it is further convenient to replace the $\sin\alpha$ in this expression by $\sin\alpha'$. Since we have not

considered overhangs, slanted cliffs, etc., $\sin\alpha/\cos i$ can only
be considered a first approximation to the correct expression
anyway.

Our final expression for the infrared radiance of the
lunar surface is

$$B(i,\epsilon,\alpha) = \frac{a_1\cos i + a_2\cos\alpha'}{1+a_4\sin\alpha'/\cos i} + a_3\{(\pi-|\alpha|)\cos|\alpha|+\sin|\alpha|\}/\pi \qquad (10)$$

with α' given by Equation (6).

The argument we have given, leading to Equation (10) can
certainly not be considered anything more than a crude heuristic
argument. However as will be seen, by proper choice of the
parameters a_1, a_2, a_3 and a_4, quite an accurate fit to the available
infrared data can be obtained, for the whole moon under all
conditions of illumination and observation.

Four adjustable parameters may seem like quite a few;
however from the known incident energy, one condition is obtained
connecting a_1, a_2, and a_3. The constant a_4, according to our
argument, should be determined in principle by the ratio of
heights of large cliffs or peaks to the distances between them.
The number of more-or-less spherically shaped rocks on the flat
surfaces should determine a_3, and finally the directional character-
istics of the term $a_2\cos\alpha'$ should be due to directional emission
from the bottoms of small craters on the more-or-less flat

s.

With these qualitative interpretations of the various terms, we now shall discuss the fit of Equation (10) to the data. We obtained a large number of data on radiance from the observations of Pettit and Nicholson, Sinton, and Saari and Shorthill, and ran a least squares analysis to determine $a_i (i = 1,2,3,4)$. The values so determined gave an rms error of about .05 $cal/cm^2 min$. The actual values of a_2, a_3, a_4 all are rather small compared to a_1, and the rms error does not change significantly if a_2, a_3, a_4 are varied by 50% or so. Therfore we made further adjustments of a_2, a_3, and a_4 to obtain better fits to certain selected data.

One datum of considerable reliability is the integrated energy from the subsolar point, 1.88 $cal/cm^2 min$.[4] Using the fact that a_2, a_3, a_4 are all small compared to a_1, requiring the integrated energy to have this value gives the condition

$$0.2992 = \tfrac{1}{2}a_1 + \tfrac{1}{3}a_2 + 0.404a_3 - \tfrac{1}{3}a_1 a_4 + \tfrac{1}{4}a_1 a_4^2 - .1963a_2 a_4. \quad (11)$$

This condition can easily be satisfied by adjusting a_2 and a_3 slightly, without significantly changing the rms error.

The brightness distribution along the equator at full moon will be fit satisfactorily if

$$\frac{a_2 + a_3}{a_1} = .55 \quad . \qquad (12)$$

The brightness distribution along the equator at first and third quarter moons will be fit at large angles of incidence provided

$$a_3 = 0.074 \quad . \qquad (13)$$

By proceeding in a similar way, one can obtain a number of conditions on the parameters to obtain good fits in the north-south direction at full moon or quarter moon, or at some chosen point such as the subsolar point, and so forth. These conditions are not all consistent, reflecting the fact that Equation (10) is not a perfect expression for the emitted radiation.

After examination of the available data, we have selected the following values of the parameters a_1, a_2, a_3, a_4 for which (10) best represents the lunar infrared radiation under all conditions:

$$a_1 = 0.481 \text{ cal/cm}^2\text{min}$$

$$a_2 = 0.140 \text{ cal/cm}^2\text{min}$$

$$a_3 = 0.074 \text{ cal/cm}^2\text{min}$$

$$a_4 = 0.121 \tag{14}$$

These give a net rms error of .052 cal/cm^{2}min. Generally if one of the constants is changed to produce a better fit of some selected subset of the data, the agreement will be made worse somewhere else.

Comparison with experiment

In Figures 4, 5, 6, and 7 we give comparisons of the calculated energy with experimental data for certain selected cases which we believe gives a fair idea of how well Equation (10) agrees with experiment.

In Figure 4 values of $\pi B(0, \epsilon, \epsilon)$ are plotted as a function of ϵ, together with data obtained from Sinton[2] and Pettit and

Nicholson.[1] The agreement is satisfatory in view of the wide

scatter in the data, except possibly at very large ϵ (near 90°)

where it may be possibly not decrease rapdily enough. We note

also that the data points taken from Pettit and Nicholson[1] are

subject to a calibration error and should be corrected downwards

by about 9%.[4] A reasonably good fit at the subsolar point is

desirable since the quantity of energy involved (1.88 cal/cm^{2}min)

is greater there than at any other point on the moon.

In Figure 5, the calculated brightness temperatures along

the equator at first and third quarter moons are compared with

experiment. The agreement is quite good. The limiting value of

173° for the brightness temperature at the terminator is obtained,

due to the presence of the term involving a_3 in Equation (10).

In Figure 6, the theoretical expression is compared with

observations at full moon along the equator and in the north-

south directions. Agreement along the equator is very good; in

the north-south directions however, the calculated brightness is

a few degrees too high. Agreement here could be improved by

different choices of $a_i (i=1,2,3,4)$ but would suffer elsewhere.

We note the large deviation of the data from the $\cos^{1/6}\theta$ law

proposed by Pettit and Nicholson. Our expression at full moon

reduces to

$$B(i,i,0) = a_1 \cos i + a_2 + a_3 \qquad (15)$$

$(i=\theta)$ which is in quite good agreement with observation.
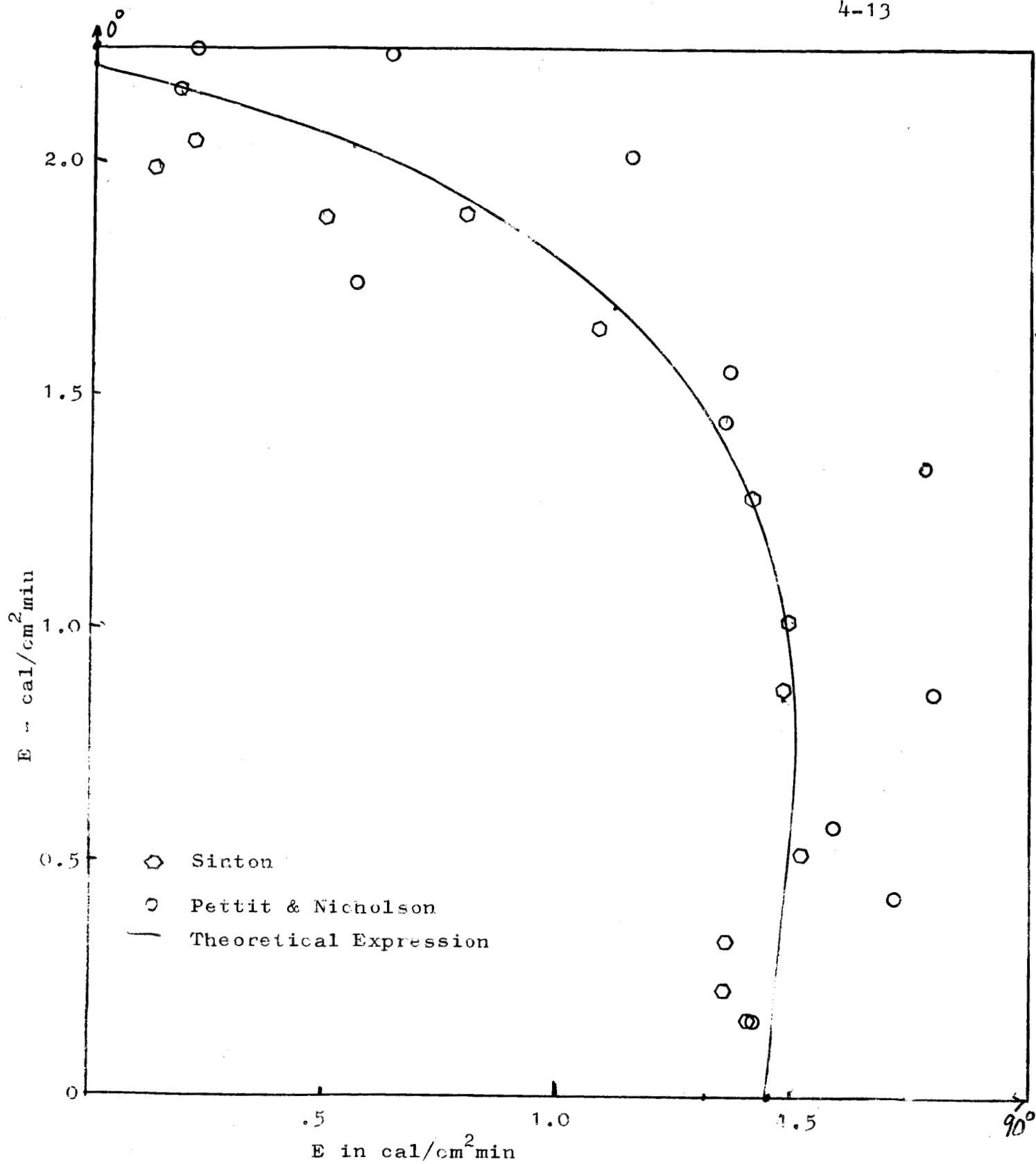
Figure 4: Polar plot of lunar heat from the subsolar point as a function of angle of observation.
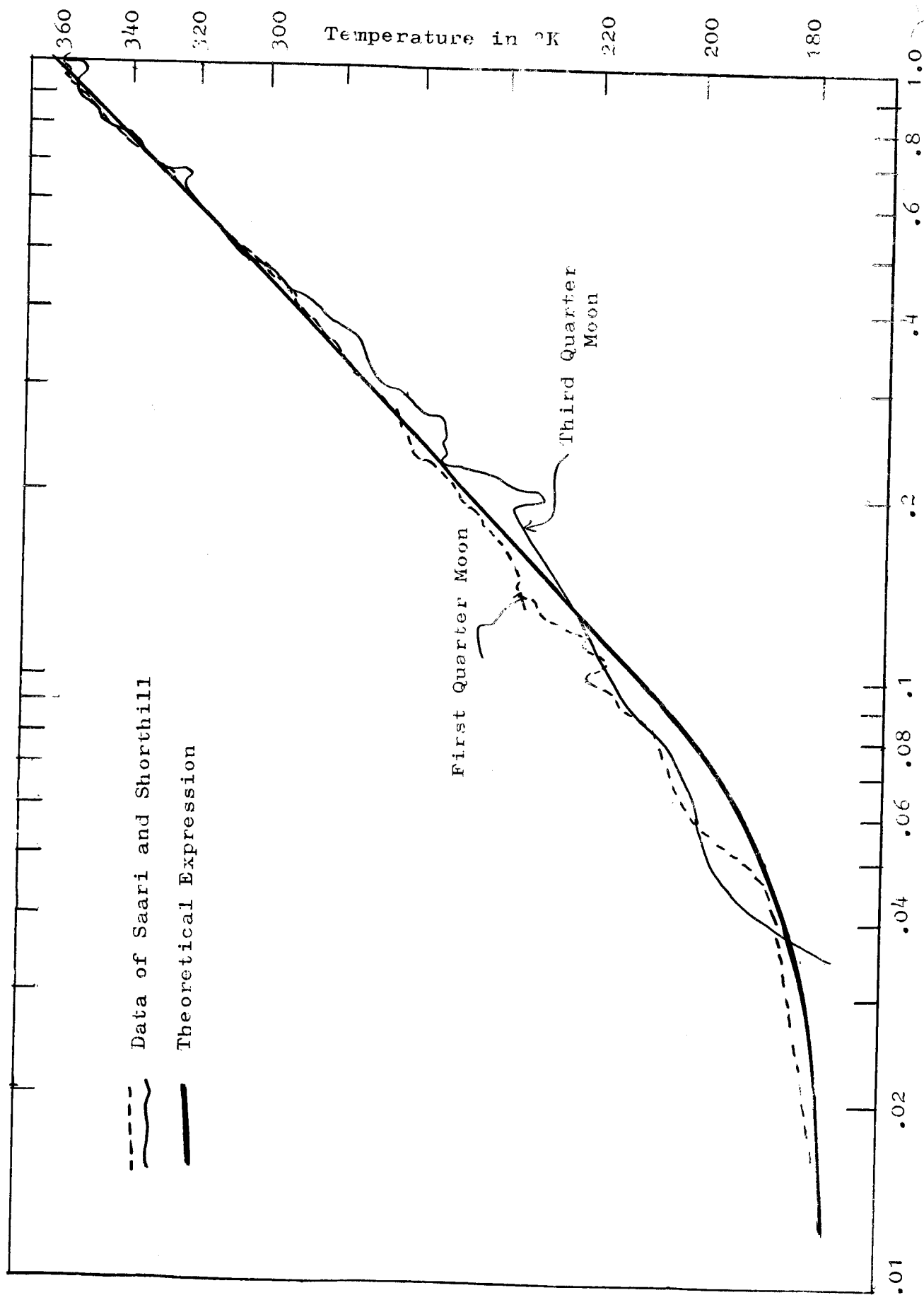
Figure 5: Brightness temperature values along the equator for first and third quarter moons, compared with theoretical expression.
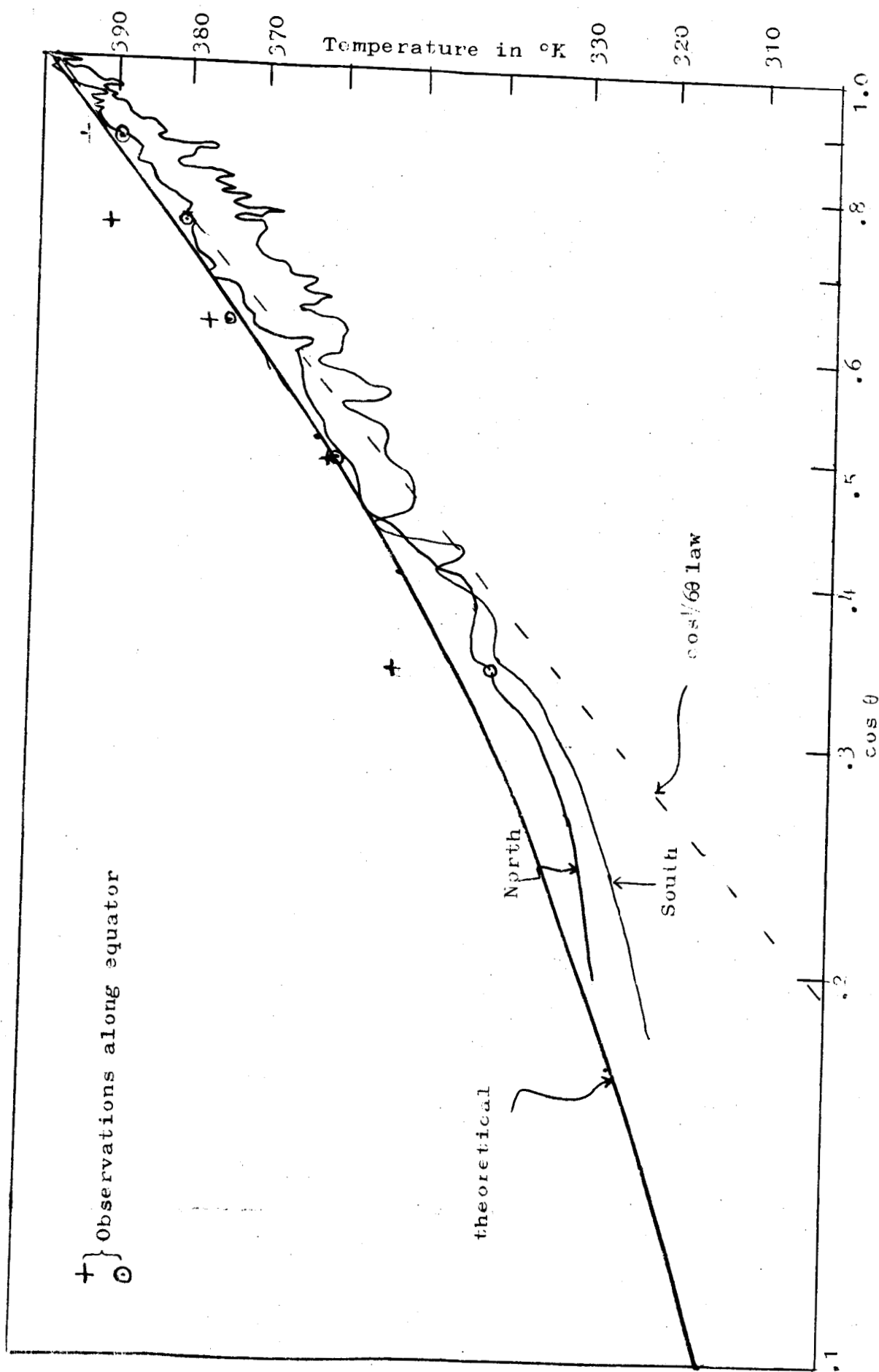
Figure 6: Comparison of observations at full moon in north-south directions and along equator, with theoretical expression.

In Figure 7 we have plotted the calculated brightness
temperature versus observation for another extreme case, an angle
of incidence 80°, at various angles of observation, along the
lunar equator. The agreement is satisfactory.

In Appendix IV-A, complete tables of the infrared brightness,
determined by Equations (10) and (14), are given.

Table 4-1 gives our results on a check of energy balance
at a position at which the angle of incidence is i. Column 1
conta ns the heat energy integrated over all angles. Column 2
contains the average reflected energy at this position assuming
a mean normal albedo of .105 and a mean compaction parameter of
.50. In the third column is the total energy leaving the lunar
surface. The last column is the available energy, $S_0\cos i$, and
should compare with the energy in column 4. The agreement is
seen to be reasonably good.

Conclusions

A mathematical expression has been presented which repre-
sents reasonably well the infrared component of lunar radiation
under almost all conditions of illumination and observation. The
lunar infrared radiation may be considered as due mainly to
black-body radiation (following Lambert's law), since the
coefficient a_1 is so large compared to the other parameters.
There are in addition directional components, which are peaked
back toward the sun in the direction $\alpha = 0$. These are probably

Figure 22 Comparison of Experimental and Theoretical Brightness Temperatures along Equator. (Angle of incidence = 80°)(Evening sun)

⊙ Brightness Temperature from Saari and Shorthill data

—— Theoretical Expression
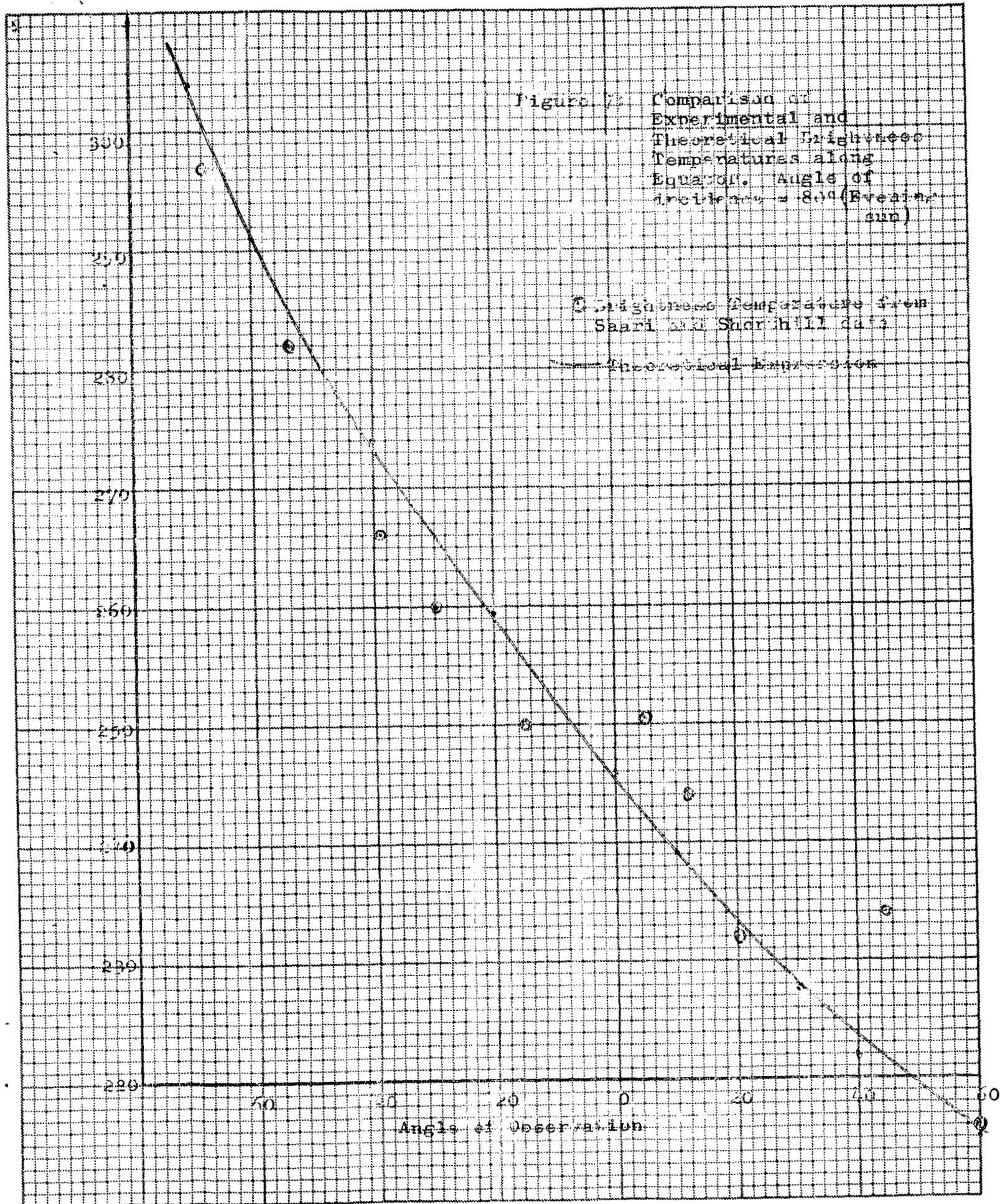
Table 4-1

Test of Energy Balance on the Lunar Surface

Angle of Incidence	Integrated Infrared Energy (cal/cm²min)	Integrated Reflected Energy (cal/cm²min)	Average Heat Conducted away from Surface (cal/cm²min)	Sum of Preceeding Columns	$S_o \cos i$
0°	1.87	.096	.010	1.98	1.99
5°	1.86	.096	.010	1.97	1.98
10°	1.84	.095	.011	1.95	1.96
15°	1.81	.093	.011	1.91	1.92
20°	1.77	.091	.011	1.87	1.87
25°	1.71	.088	.012	1.81	1.80
30°	1.63	.085	.012	1.73	1.72
35°	1.55	.081	.012	1.64	1.63
40°	1.45	.076	.012	1.54	1.52
45°	1.34	.071	.012	1.42	1.41
50°	1.23	.065	.011	1.31	1.28
55°	1.10	.059	.010	1.17	1.14
60°	.967	.0516	.001	1.03	1.00
65°	.826	.0437	.007	.88	.84
70°	.681	.0352	.006	.72	.681
75°	.532	.0260	.004	.56	.515
80°	.380	.0162	.001	.40	.346
85°	.230	.0063	-.001	.24	.173

due to features such as rocks or domes which shadow themselves, the illuminated portions following Lambert's law, to high cliffs or peaks which cast long shadows, and to directional radiation from the bottoms of the craters.

We have not given a complete model of the rough surface, but have more or less invented an expression which fits the data. Further work in this problem should probably consider more in detail the radiation from such rough surface features, with a view to improving the mathematical form of the contributions due to directional components, which has been expressed through the (reasonable) expression (7) and the (highly artificial) expression (6). The effect of shadowing as expressed in Equation (4) is probably not too far off.

Table 4-2

Heat conducted away from Lunar Surface in units of cal/cm²min.

Explanation of table: The energies are calculated using the formula derived by Sinton,[2]

$$F_o = -\left(\frac{2\pi}{p}\right)^{\frac{1}{2}} (k\rho c)^{\frac{1}{2}} \sum_{n=0}^{3} \sqrt{n}\ T_n \cos(2\pi n\theta + \epsilon_n + \pi/n)$$

where $(k\rho c)^{\frac{1}{2}} = .001$ is the thermal inertia, P is the period of the moon in sec, and T_n and ϵ_n are given as follows:

$$T_0 = 210°K \qquad \epsilon_0 = 0$$

$$T_1 = 157°K \qquad \epsilon_1 = -6°$$

$$T_2 = 34°K \qquad \epsilon_2 = +6$$

$$T_3 = 30°K \qquad \epsilon_3 = +159$$

The angle θ is measured from the subsolar point. Only values along the equator are given, with θ varying from $-180°$ at lunar midnight, through morning and evening back to $+180°$ at midnight. F_o is in cal/cm²min.

θ	F_o	θ	F_o
$-180°$	$-.0044$	$-130°$	$-.0095$
$-175°$	$-.0049$	$-125°$	$-.0085$
$-170°$	$-.0056$	$-120°$	$-.0070$
$-165°$	$-.0065$	$-115°$	$-.0050$
$-160°$	$-.0075$	$-110°$	$-.0026$
$-155°$	$-.0085$	$-105°$	$-.0000$
$-150°$	$-.0094$	$-100°$	$+.0029$
$-145°$	$-.0100$	$-95°$	$+.0059$
$-140°$	$-.0102$	$-90°$	$+.0088$
$-135°$	$-.0101$	$-85°$	$.0117$

Table 4-2 (Continued)

θ	F_o	θ	F_o
-80°	.0143	55°	-.0005
-75°	.0166	60°	-.0024
-70°	.0185	65°	-.0045
-65°	.0199	70°	-.0067
-60°	.0209	75°	-.0089
-55°	.0214	80°	-.0111
-50°	.0214	85°	-.0130
-45°	.0210	90°	-.0148
-40°	.0202	95°	-.0163
-35°	.0192	100°	-.0174
-30°	.0179	105°	-.0181
-25°	.0166	110°	-.0183
-20°	.0152	115°	-.0181
-15°	.0138	120°	-.0175
-10°	.0125	125°	-.0165
- 5°	.0114	130°	-.0151
0°	.0104	135°	-.0136
5°	.0095	140°	-.0119
10°	.0087	145°	-.0101
15°	.0080	150°	-.0085
20°	.0074	155°	-.0071
25°	.0067	160°	-.0059
30°	.0059	165°	-.0049
35°	.0051	170°	-.0044
40°	.0040	175°	-.0042
45°	.0027	180°	-.0044
50°	.0012		

REFERENCES FOR CHAPTER IV

1. E. Pettit and S. B. Nicholson, Ap. J. 71, 102 (1930).

2. W. M. Sinton, "Temperatures on the Lunar Surface," Ch. 11 in
    Physics and Astronomy of the Moon, Ed. by Z. Kopal, Academic
    Press, 1962, p. 417.

3. C. G. Montgomery, J. M. Saari, R. W. Shorthill, N. F, Six,
    Jr., "Directional Characteristics of Lunar Thermal Emission,"
    Technical Note R-213, Brown Engineering Company, November,
    1966.

4. N. Ashby, Publ. Astr. Soc. Pac. 78, No. 461, 254 (1966).

APPENDIX IV-A

Calculated Emitted Energies from the Lunar Surface

Angle of Incidence	Angle of Observation	Azimuthal Angle Between Incident & Observed Ray	Magnitude of Phase Angle	Energy in Cal/cm^2 per min/ Steradian
80.0	0.0	0.0	80.0	0.0945
80.0	5.0	0.0	85.0	0.0895
80.0	10.0	0.0	90.0	0.0848
80.0	15.0	0.0	95.0	0.0805
80.0	20.0	0.0	100.0	0.0764
80.0	25.0	0.0	105.0	0.0726
80.0	30.0	0.0	110.0	0.0692
80.0	35.0	0.0	115.0	0.0661
80.0	40.0	0.0	120.0	0.0633
80.0	45.0	0.0	125.0	0.0608
80.0	50.0	0.0	130.0	0.0586
80.0	55.0	0.0	135.0	0.0566
80.0	60.0	0.0	140.0	0.0550
80.0	65.0	0.0	145.0	0.0536
80.0	70.0	0.0	150.0	0.0524
80.0	75.0	0.0	155.0	0.0514
80.0	80.0	0.0	160.0	0.0506
80.0	85.0	0.0	165.0	0.0500
80.0	0.0	15.0	80.0	0.0945
80.0	5.0	15.0	84.8	0.0897
80.0	10.0	15.0	89.7	0.0851
80.0	15.0	15.0	94.5	0.0809
80.0	20.0	15.0	99.3	0.0769
80.0	25.0	15.0	104.2	0.0732
80.0	30.0	15.0	109.0	0.0698
80.0	35.0	15.0	113.8	0.0667
80.0	40.0	15.0	118.6	0.0639
80.0	45.0	15.0	123.4	0.0614
80.0	50.0	15.0	128.1	0.0592
80.0	55.0	15.0	132.8	0.0572
80.0	60.0	15.0	137.5	0.0555
80.0	65.0	15.0	142.1	0.0541
80.0	70.0	15.0	146.6	0.0528
80.0	75.0	15.0	150.9	0.0518
80.0	80.0	15.0	155.0	0.0509
80.0	85.0	15.0	158.8	0.0502
80.0	0.0	30.0	80.0	0.0945
80.0	5.0	30.0	84.3	0.0902

APPENDIX IV-A (Continued)

Angle of Incidence	Angle of Observation	Azimuthal Angle, etc.	Magnitude of Phase Angle	Energy in Cal/cm^2 per min/ Steradian
80.0	10.0	30.0	88.7	0.0860
80.0	15.0	30.0	93.0	0.0820
80.0	20.0	30.0	97.4	0.0783
80.0	25.0	30.0	101.7	0.0748
80.0	30.0	30.0	106.0	0.0715
80.0	35.0	30.0	110.3	0.0685
80.0	40.0	30.0	114.5	0.0658
80.0	45.0	30.0	118.7	0.0633
80.0	50.0	30.0	122.8	0.0611
80.0	55.0	30.0	126.8	0.0591
80.0	60.0	30.0	130.7	0.0573
80.0	65.0	30.0	134.4	0.0557
80.0	70.0	30.0	137.9	0.0544
80.0	75.0	30.0	141.2	0.0532
80.0	80.0	30.0	144.1	0.0522
80.0	85.0	30.0	146.6	0.0514
80.0	0.0	45.0	80.0	0.0945
80.0	5.0	45.0	83.6	0.0909
80.0	10.0	45.0	87.1	0.0874
80.0	15.0	45.0	90.7	0.0839
80.0	20.0	45.0	94.3	0.0806
80.0	25.0	45.0	97.9	0.0775
80.0	30.0	45.0	101.4	0.0745
80.0	35.0	45.0	104.9	0.0717
80.0	40.0	45.0	108.3	0.0691
80.0	45.0	45.0	111.7	0.0667
80.0	50.0	45.0	115.0	0.0645
80.0	55.0	45.0	118.1	0.0624
80.0	60.0	45.0	121.1	0.0606
80.0	65.0	45.0	123.9	0.0589
80.0	70.0	45.0	126.5	0.0575
80.0	75.0	45.0	128.9	0.0562
80.0	80.0	45.0	131.0	0.0550
80.0	85.0	45.0	132.7	0.0540
80.0	0.0	60.0	80.0	0.0945
80.0	5.0	60.0	82.5	0.0919
80.0	10.0	60.0	85.1	0.0892
80.0	15.0	60.0	87.7	0.0866
80.0	20.0	60.0	90.3	0.0839
80.0	25.0	60.0	92.9	0.0813
80.0	30.0	60.0	95.5	0.0787
80.0	35.0	60.0	98.1	0.0763
80.0	40.0	60.0	100.6	0.0739

APPENDIX IV-A (Continued)

Angle of Incidence	Angle of Observation	Azimuthal Angle, etc.	Magnitude of Phase Angle	Energy in Cal/cm^2 per min/ Steradian
80.0	45.0	60.0	103.0	0.0717
80.0	50.0	60.0	105.4	0.0696
80.0	55.0	60.0	107.7	0.0676
80.0	60.0	60.0	109.9	0.0657
80.0	65.0	60.0	111.9	0.0640
80.0	70.0	60.0	113.8	0.0625
80.0	75.0	60.0	115.5	0.0611
80.0	80.0	60.0	117.1	0.0598
80.0	85.0	60.0	118.4	0.0587
80.0	0.0	75.0	80.0	0.0945
80.0	5.0	75.0	81.3	0.0931
80.0	10.0	75.0	82.7	0.0915
80.0	15.0	75.0	84.2	0.0898
80.0	20.0	75.0	85.6	0.0880
80.0	25.0	75.0	87.2	0.0861
80.0	30.0	75.0	88.7	0.0841
80.0	35.0	75.0	90.2	0.0822
80.0	40.0	75.0	91.8	0.0802
80.0	45.0	75.0	93.3	0.0783
80.0	50.0	75.0	94.8	0.0765
80.0	55.0	75.0	96.3	0.0746
80.0	60.0	75.0	97.7	0.0729
80.0	65.0	75.0	99.1	0.0712
80.0	70.0	75.0	100.4	0.0696
80.0	75.0	75.0	101.6	0.0682
80.0	80.0	75.0	102.8	0.0668
80.0	85.0	75.0	103.8	0.0655
80.0	0.0	90.0	80.0	0.0945
80.0	5.0	90.0	80.0	0.0944
80.0	10.0	90.0	80.2	0.0940
80.0	15.0	90.0	80.3	0.0935
80.0	20.0	90.0	80.6	0.0927
80.0	25.0	90.0	80.9	0.0918
80.0	30.0	90.0	81.4	0.0907
80.0	35.0	90.0	81.8	0.0894
80.0	40.0	90.0	82.4	0.0881
80.0	45.0	90.0	82.9	0.0866
80.0	50.0	90.0	83.6	0.0851
80.0	55.0	90.0	84.3	0.0836
80.0	60.0	90.0	85.0	0.0820
80.0	65.0	90.0	85.8	0.0805
80.0	70.0	90.0	86.6	0.0789
80.0	75.0	90.0	87.4	0.0774

APPENDIX IV-A (Continued)

Angle of Incidence	Angle of Observation	Azimuthal Angle, etc.	Magnitude of Phase Angle	Energy in Cal/cm^2 per min/ Steradian
80.0	80.0	90.0	88.3	0.0759
80.0	85.0	90.0	89.1	0.0744
80.0	0.0	105.0	80.0	0.0945
80.0	5.0	105.0	78.7	0.0957
80.0	10.0	105.0	77.6	0.0967
80.0	15.0	105.0	76.5	0.0975
80.0	20.0	105.0	75.5	0.0980
80.0	25.0	105.0	74.6	0.0982
80.0	30.0	105.0	73.9	0.0981
80.0	35.0	105.0	73.2	0.0978
80.0	40.0	105.0	72.7	0.0973
80.0	45.0	105.0	72.4	0.0965
80.0	50.0	105.0	72.1	0.0955
80.0	55.0	105.0	72.0	0.0943
80.0	60.0	105.0	72.1	0.0930
80.0	65.0	105.0	72.3	0.0916
80.0	70.0	105.0	72.6	0.0900
80.0	75.0	105.0	73.1	0.0884
80.0	80.0	105.0	73.7	0.0867
80.0	85.0	105.0	74.4	0.0849
80.0	0.0	120.0	80.0	0.0945
80.0	5.0	120.0	77.5	0.0970
80.0	10.0	120.0	75.1	0.0994
80.0	15.0	120.0	72.8	0.1015
80.0	20.0	120.0	70.6	0.1034
80.0	25.0	120.0	68.6	0.1050
80.0	30.0	120.0	66.6	0.1063
80.0	35.0	120.0	64.9	0.1072
80.0	40.0	120.0	63.3	0.1077
80.0	45.0	120.0	61.9	0.1077
80.0	50.0	120.0	60.7	0.1074
80.0	55.0	120.0	59.8	0.1067
80.0	60.0	120.0	59.1	0.1057
80.0	65.0	120.0	58.7	0.1043
80.0	70.0	120.0	58.5	0.1027
80.0	75.0	120.0	58.6	0.1008
80.0	80.0	120.0	59.0	0.0987
80.0	85.0	120.0	59.6	0.0965
80.0	0.0	135.0	80.0	0.0945
80.0	5.0	135.0	76.5	0.0981
80.0	10.0	135.0	73.0	0.1017
80.0	15.0	135.0	69.6	0.1053
80.0	20.0	135.0	66.3	0.1086

APPENDIX IV-A (Continued)

Angle of Incidence	Angle of Observation	Azimuthal Angle, etc.	Magnitude of Phase Angle	Energy in Cal/cm^2 per min/ Steradian
80.0	25.0	135.0	63.1	0.1118
80.0	30.0	135.0	60.1	0.1146
80.0	35.0	135.0	57.2	0.1171
80.0	40.0	135.0	54.5	0.1190
80.0	45.0	135.0	52.0	0.1204
80.0	50.0	135.0	49.8	0.1211
80.0	55.0	135.0	47.9	0.1211
80.0	60.0	135.0	46.4	0.1205
80.0	65.0	135.0	45.2	0.1191
80.0	70.0	135.0	44.5	0.1171
80.0	75.0	135.0	44.1	0.1146
80.0	80.0	135.0	44.3	0.1116
80.0	85.0	135.0	44.9	0.1083
80.0	0.0	150.0	80.0	0.0945
80.0	5.0	150.0	75.7	0.0990
80.0	10.0	150.0	71.4	0.1036
80.0	15.0	150.0	67.1	0.1084
80.0	20.0	150.0	62.9	0.1131
80.0	25.0	150.0	58.8	0.1178
80.0	30.0	150.0	54.8	0.1224
80.0	35.0	150.0	50.8	0.1267
80.0	40.0	150.0	47.1	0.1307
80.0	45.0	150.0	43.5	0.1342
80.0	50.0	150.0	40.1	0.1369
80.0	55.0	150.0	37.0	0.1386
80.0	60.0	150.0	34.4	0.1391
80.0	65.0	150.0	32.2	0.1383
80.0	70.0	150.0	30.6	0.1359
80.0	75.0	150.0	29.7	0.1320
80.0	80.0	150.0	29.5	0.1268
80.0	85.0	150.0	30.1	0.1206
80.0	0.0	165.0	80.0	0.0945
80.0	5.0	165.0	75.2	0.0996
80.0	10.0	165.0	70.4	0.1049
80.0	15.0	165.0	65.5	0.1104
80.0	20.0	165.0	60.8	0.1161
80.0	25.0	165.0	56.0	0.1221
80.0	30.0	165.0	51.2	0.1282
80.0	35.0	165.0	46.5	0.1344
80.0	40.0	165.0	41.9	0.1408
80.0	45.0	165.0	37.3	0.1473
80.0	50.0	165.0	32.8	0.1536
80.0	55.0	165.0	28.5	0.1597

APPENDIX IV-A (Continued)

Angle of Incidence	Angle of Observation	Azimuthal Angle, etc.	Magnitude of Phase Angle	Energy in Cal/cm^2 per min/ Steradian
80.0	60.0	165.0	24.4	0.1651
80.0	65.0	165.0	20.7	0.1689
80.0	70.0	165.0	17.6	0.1699
80.0	75.0	165.0	15.5	0.1663
80.0	80.0	165.0	14.8	0.1566
80.0	85.0	165.0	15.7	0.1406
80.0	0.0	180.0	80.0	0.0945
80.0	5.0	180.0	75.0	0.0998
80.0	10.0	180.0	70.0	0.1053
80.0	15.0	180.0	65.0	0.1111
80.0	20.0	180.0	60.0	0.1172
80.0	25.0	180.0	55.0	0.1237
80.0	30.0	180.0	50.0	0.1304
80.0	35.0	180.0	45.0	0.1375
80.0	40.0	180.0	40.0	0.1451
80.0	45.0	180.0	35.0	0.1534
80.0	50.0	180.0	30.0	0.1625
80.0	55.0	180.0	25.0	0.1728
80.0	60.0	180.0	20.0	0.1850
80.0	65.0	180.0	15.0	0.2001
80.0	70.0	180.0	10.0	0.2201
80.0	75.0	180.0	5.0	0.2493
80.0	80.0	180.0	0.0	0.2975
80.0	85.0	180.0	5.0	0.2235
60.0	0.0	0.0	60.0	0.3021
60.0	5.0	0.0	65.0	0.2925
60.0	10.0	0.0	70.0	0.2834
60.0	15.0	0.0	75.0	0.2746
60.0	20.0	0.0	80.0	0.2663
60.0	25.0	0.0	85.0	0.2585
60.0	30.0	0.0	90.0	0.2511
60.0	35.0	0.0	95.0	0.2441
60.0	40.0	0.0	100.0	0.2376
60.0	45.0	0.0	105.0	0.2316
60.0	50.0	0.0	110.0	0.2259
60.0	55.0	0.0	115.0	0.2207
60.0	60.0	0.0	120.0	0.2159
60.0	65.0	0.0	125.0	0.2115
60.0	70.0	0.0	130.0	0.2075
60.0	75.0	0.0	135.0	0.2039
60.0	80.0	0.0	140.0	0.2006
60.0	85.0	0.0	145.0	0.1977
60.0	0.0	15.0	60.0	0.3021

APPENDIX IV-A (Continued)

Angle of Incidence	Angle of Observation	Azimuthal Angle, etc.	Magnitude of Phase Angle	Energy in Cal/cm^2 per min/ Steradian
60.0	5.0	15.0	64.8	0.2928
60.0	10.0	15.0	69.7	0.2839
60.0	15.0	15.0	74.5	0.2753
60.0	20.0	15.0	79.4	0.2671
60.0	25.0	15.0	84.3	0.2594
60.0	30.0	15.0	89.2	0.2520
60.0	35.0	15.0	94.0	0.2451
60.0	40.0	15.0	98.9	0.2386
60.0	45.0	15.0	103.8	0.2325
60.0	50.0	15.0	108.6	0.2269
60.0	55.0	15.0	113.5	0.2216
60.0	60.0	15.0	118.3	0.2168
60.0	65.0	15.0	123.1	0.2123
60.0	70.0	15.0	128.0	0.2083
60.0	75.0	15.0	132.7	0.2046
60.0	80.0	15.0	137.5	0.2012
60.0	85.0	15.0	142.2	0.1982
60.0	0.0	30.0	60.0	0.3021
60.0	5.0	30.0	64.4	0.2937
60.0	10.0	30.0	68.8	0.2854
60.0	15.0	30.0	73.2	0.2773
60.0	20.0	30.0	77.7	0.2696
60.0	25.0	30.0	82.2	0.2621
60.0	30.0	30.0	86.7	0.2549
60.0	35.0	30.0	91.2	0.2481
60.0	40.0	30.0	95.7	0.2416
60.0	45.0	30.0	100.2	0.2355
60.0	50.0	30.0	104.7	0.2298
60.0	55.0	30.0	109.1	0.2244
60.0	60.0	30.0	113.5	0.2194
60.0	65.0	30.0	117.9	0.2148
60.0	70.0	30.0	122.3	0.2105
60.0	75.0	30.0	126.5	0.2066
60.0	80.0	30.0	130.7	0.2030
60.0	85.0	30.0	134.7	0.1998
60.0	0.0	45.0	60.0	0.3021
60.0	5.0	45.0	63.6	0.2951
60.0	10.0	45.0	67.3	0.2879
60.0	15.0	45.0	71.1	0.2807
60.0	20.0	45.0	74.9	0.2736
60.0	25.0	45.0	78.8	0.2666
60.0	30.0	45.0	82.7	0.2597
60.0	35.0	45.0	86.7	0.2531

APPENDIX IV-A (Continued)

Angle of Incidence	Angle of Observation	Azimuthal Angle,etc.	Magnitude of Phase Angle	Energy in Cal/cm^2 per min/ Steradian
60.0	40.0	45.0	90.6	0.2467
60.0	45.0	45.0	94.6	0.2406
60.0	50.0	45.0	98.5	0.2348
60.0	55.0	45.0	102.4	0.2293
60.0	60.0	45.0	106.3	0.2241
60.0	65.0	45.0	110.1	0.2192
60.0	70.0	45.0	113.9	0.2146
60.0	75.0	45.0	117.5	0.2104
60.0	80.0	45.0	121.1	0.2064
60.0	85.0	45.0	124.5	0.2028
60.0	0.0	60.0	60.0	0.3021
60.0	5.0	60.0	62.6	0.2970
60.0	10.0	60.0	65.3	0.2913
60.0	15.0	60.0	68.2	0.2854
60.0	20.0	60.0	71.2	0.2792
60.0	25.0	60.0	74.3	0.2729
60.0	30.0	60.0	77.5	0.2666
60.0	35.0	60.0	80.7	0.2603
60.0	40.0	60.0	84.0	0.2541
60.0	45.0	60.0	87.3	0.2481
60.0	50.0	60.0	90.6	0.2422
60.0	55.0	60.0	93.9	0.2365
60.0	60.0	60.0	97.2	0.2310
60.0	65.0	60.0	100.4	0.2258
60.0	70.0	60.0	103.6	0.2209
60.0	75.0	60.0	106.8	0.2162
60.0	80.0	60.0	109.9	0.2118
60.0	85.0	60.0	112.8	0.2076
60.0	0.0	75.0	60.0	0.3021
60.0	5.0	75.0	61.4	0.2992
60.0	10.0	75.0	63.0	0.2955
60.0	15.0	75.0	64.9	0.2912
60.0	20.0	75.0	66.8	0.2864
60.0	25.0	75.0	69.0	0.2812
60.0	30.0	75.0	71.3	0.2756
60.0	35.0	75.0	73.7	0.2699
60.0	40.0	75.0	76.2	0.2640
60.0	45.0	75.0	78.8	0.2581
60.0	50.0	75.0	81.4	0.2521
60.0	55.0	75.0	84.1	0.2463
60.0	60.0	75.0	86.8	0.2405
60.0	65.0	75.0	89.5	0.2349
60.0	70.0	75.0	92.3	0.2294

APPENDIX IV-A (Continued)

Angle of Incidence	Angle of Observation	Azimuthal Angle,etc.	Magnitude of Phase Angle	Energy in Cal/cm^2 per min/ Steradian
60.0	75.0	75.0	95.0	0.2242
60.0	80.0	75.0	97.7	0.2192
60.0	85.0	75.0	100.4	0.2144
60.0	0.0	90.0	60.0	0.3021
60.0	5.0	90.0	60.1	0.3017
60.0	10.0	90.0	60.5	0.3003
60.0	15.0	90.0	61.1	0.2981
60.0	20.0	90.0	62.0	0.2950
60.0	25.0	90.0	63.1	0.2913
60.0	30.0	90.0	64.3	0.2869
60.0	35.0	90.0	65.8	0.2820
60.0	40.0	90.0	67.5	0.2766
60.0	45.0	90.0	69.3	0.2710
60.0	50.0	90.0	71.3	0.2651
60.0	55.0	90.0	73.3	0.2590
60.0	60.0	90.0	75.5	0.2529
60.0	65.0	90.0	77.8	0.2467
60.0	70.0	90.0	80.2	0.2406
60.0	75.0	90.0	82.6	0.2346
60.0	80.0	90.0	85.0	0.2287
60.0	85.0	90.0	87.5	0.2230
60.0	0.0	105.0	60.0	0.3021
60.0	5.0	105.0	58.8	0.3043
60.0	10.0	105.0	57.9	0.3055
60.0	15.0	105.0	57.2	0.3057
60.0	20.0	105.0	56.9	0.3049
60.0	25.0	105.0	56.8	0.3032
60.0	30.0	105.0	57.0	0.3004
60.0	35.0	105.0	57.4	0.2968
60.0	40.0	105.0	58.2	0.2924
60.0	45.0	105.0	59.2	0.2872
60.0	50.0	105.0	60.5	0.2814
60.0	55.0	105.0	61.9	0.2752
60.0	60.0	105.0	63.6	0.2686
60.0	65.0	105.0	65.5	0.2617
60.0	70.0	105.0	67.6	0.2546
60.0	75.0	105.0	69.8	0.2475
60.0	80.0	105.0	72.1	0.2403
60.0	85.0	105.0	74.5	0.2333
60.0	0.0	120.0	60.0	0.3021
60.0	5.0	120.0	57.6	0.3067
60.0	10.0	120.0	55.4	0.3106
60.0	15.0	120.0	53.5	0.3136

APPENDIX IV-A (Continued)

Angle of Incidence	Angle of Observation	Azimuthal Angle,etc.	Magnitude of Phase Angle	Energy in Cal/cm^2 per min/ Steradian
60.0	20.0	120.0	51.8	0.3156
60.0	25.0	120.0	50.5	0.3165
60.0	30.0	120.0	49.5	0.3161
60.0	35.0	120.0	48.9	0.3145
60.0	40.0	120.0	48.6	0.3116
60.0	45.0	120.0	48.7	0.3075
60.0	50.0	120.0	49.2	0.3022
60.0	55.0	120.0	50.1	0.2958
60.0	60.0	120.0	51.3	0.2886
60.0	65.0	120.0	52.9	0.2807
60.0	70.0	120.0	54.7	0.2722
60.0	75.0	120.0	56.8	0.2633
60.0	80.0	120.0	59.1	0.2542
60.0	85.0	120.0	61.6	0.2449
60.0	0.0	135.0	60.0	0.3021
60.0	5.0	135.0	56.5	0.3089
60.0	10.0	135.0	53.2	0.3154
60.0	15.0	135.0	50.1	0.3212
60.0	20.0	135.0	47.2	0.3264
60.0	25.0	135.0	44.6	0.3305
60.0	30.0	135.0	42.3	0.3334
60.0	35.0	135.0	40.5	0.3349
60.0	40.0	135.0	39.0	0.3347
60.0	45.0	135.0	38.1	0.3326
60.0	50.0	135.0	37.8	0.3287
60.0	55.0	135.0	38.0	0.3228
60.0	60.0	135.0	38.7	0.3152
60.0	65.0	135.0	40.0	0.3059
60.0	70.0	135.0	41.7	0.2953
60.0	75.0	135.0	43.9	0.2835
60.0	80.0	135.0	46.4	0.2710
60.0	85.0	135.0	49.2	0.2579
60.0	0.0	150.0	60.0	0.2031
60.0	5.0	150.0	55.7	0.3107
60.0	10.0	150.0	51.5	0.3193
60.0	15.0	150.0	47.4	0.3277
60.0	20.0	150.0	43.4	0.3359
60.0	25.0	150.0	39.6	0.3436
60.0	30.0	150.0	36.1	0.3506
60.0	35.0	150.0	32.9	0.3564
60.0	40.0	150.0	30.1	0.3607
60.0	45.0	150.0	27.9	0.3628
60.0	50.0	150.0	26.4	0.3624
60.0	55.0	150.0	25.7	0.3589

APPENDIX IV-A (Continued)

Angle of Incidence	Angle of Observation	Azimuthal Angle, etc.	Magnitude of Phase Angle	Energy in Cal/cm^2 per min/ Steradian
60.0	60.0	150.0	25.9	0.3520
60.0	65.0	150.0	27.0	0.3418
60.0	70.0	150.0	28.9	0.3284
60.0	75.0	150.0	31.4	0.3122
60.0	80.0	150.0	34.4	0.2936
60.0	85.0	150.0	37.7	0.2734
60.0	0.0	165.0	60.0	0.3021
60.0	5.0	165.0	55.2	0.3118
60.0	10.0	165.0	50.4	0.3218
60.0	15.0	165.0	45.6	0.3321
60.0	20.0	165.0	40.9	0.3427
60.0	25.0	165.0	36.2	0.3534
60.0	30.0	165.0	31.6	0.3642
60.0	35.0	165.0	27.2	0.3749
60.0	40.0	165.0	23.0	0.3850
60.0	45.0	165.0	19.1	0.3941
60.0	50.0	165.0	15.8	0.4010
60.0	55.0	165.0	13.6	0.4042
60.0	60.0	165.0	13.0	0.4018
60.0	65.0	165.0	14.2	0.3926
60.0	70.0	165.0	16.8	0.3766
60.0	75.0	165.0	20.4	0.3544
60.0	80.0	165.0	24.4	0.3265
60.0	85.0	165.0	28.7	0.2937
60.0	0.0	180.0	60.0	0.3021
60.0	5.0	180.0	55.0	0.3122
60.0	10.0	180.0	50.0	0.3227
60.0	15.0	180.0	45.0	0.3337
60.0	20.0	180.0	40.0	0.3451
60.0	25.0	180.0	35.0	0.3571
60.0	30.0	180.0	30.0	0.3696
60.0	35.0	180.0	25.0	0.3826.
60.0	40.0	180.0	20.0	0.3962
60.0	45.0	180.0	15.0	0.4104
60.0	50.0	180.0	10.0	0.4250
60.0	55.0	180.0	5.0	0.4398
60.0	60.0	180.0	0.0	0.4545
60.0	65.0	180.0	5.0	0.4376
60.0	70.0	180.0	10.0	0.4152
60.0	75.0	180.0	15.0	0.3865
60.0	80.0	180.0	20.0	0.3510
60.0	85.0	180.0	25.0	0.3084
30.0	0.0	0.0	30.0	0.5681
30.0	5.0	0.0	35.0	0.5559

APPENDIX IV-A (Continued)

Angle of Incidence	Angle of Observation	Azimuthal Angle,etc.	Magnitude of Phase Angle	Energy in Cal/cm^2 per min/ Steradian
30.0	10.0	0.0	40.0	0.5434
30.0	15.0	0.0	45.0	0.5309
30.0	20.0	0.0	50.0	0.5184
30.0	25.0	0.0	55.0	0.5059
30.0	30.0	0.0	60.0	0.4936
30.0	35.0	0.0	65.0	0.4816
30.0	40.0	0.0	70.0	0.4697
30.0	45.0	0.0	75.0	0.4583
30.0	50.0	0.0	80.0	0.4471
30.0	55.0	0.0	85.0	0.4364
30.0	60.0	0.0	90.0	0.4260
30.0	65.0	0.0	95.0	0.4162
30.0	70.0	0.0	100.0	0.4067
30.0	75.0	0.0	105.0	0.3978
30.0	80.0	0.0	110.0	0.3894
30.0	85.0	0.0	115.0	0.3814
30.0	0.0	15.0	30.0	0.5681
30.0	5.0	15.0	34.9	0.5562
30.0	10.0	15.0	39.7	0.5440
30.0	15.0	15.0	44.6	0.5317
30.0	20.0	15.0	49.6	0.5193
30.0	25.0	15.0	54.5	0.5070
30.0	30.0	15.0	59.4	0.4947
30.0	35.0	15.0	64.4	0.4827
30.0	40.0	15.0	69.3	0.4709
30.0	45.0	15.0	74.3	0.4594
30.0	50.0	15.0	79.2	0.4482
30.0	55.0	15.0	84.2	0.4374
30.0	60.0	15.0	89.2	0.4270
30.0	65.0	15.0	94.1	0.4171
30.0	70.0	15.0	99.1	0.4076
30.0	75.0	15.0	104.0	0.3985
30.0	80.0	15.0	109.0	0.3900
30.0	85.0	15.0	113.9	0.3819
30.0	0.0	30.0	30.0	0.5681
30.0	5.0	30.0	34.4	0.5573
30.0	10.0	30.0	39.0	0.5459
30.0	15.0	30.0	43.6	0.5342
30.0	20.0	30.0	48.3	0.5222
30.0	25.0	30.0	53.0	0.5102
30.0	30.0	30.0	57.8	0.4981
30.0	35.0	30.0	62.5	0.4862
30.0	40.0	30.0	67.4	0.4744
30.0	45.0	30.0	72.2	0.4628

APPENDIX IV-A (Continued)

Angle of Incidence	Angle of Observation	Azimuthal Angle, etc.	Magnitude of Phase Angle	Energy in Cal/cm^2 per min/ Steradian
30.0	50.0	30.0	77.0	0.4515
30.0	55.0	30.0	81.8	0.4406
30.0	60.0	30.0	86.7	0.4300
30.0	65.0	30.0	91.5	0.4198
30.0	70.0	30.0	96.4	0.4100
30.0	75.0	30.0	101.2	0.4007
30.0	80.0	30.0	106.0	0.3919
30.0	85.0	30.0	110.8	0.3835
30.0	0.0	45.0	30.0	0.5681
30.0	5.0	45.0	33.7	0.5590
30.0	10.0	45.0	37.7	0.5489
30.0	15.0	45.0	41.8	0.5382
30.0	20.0	45.0	46.1	0.5270
30.0	25.0	45.0	50.5	0.5155
30.0	30.0	45.0	55.0	0.5037
30.0	35.0	45.0	59.6	0.4920
30.0	40.0	45.0	64.1	0.4802
30.0	45.0	45.0	68.8	0.4686
30.0	50.0	45.0	73.4	0.4571
30.0	55.0	45.0	78.0	0.4459
30.0	60.0	45.0	82.7	0.4350
30.0	65.0	45.0	87.4	0.4244
30.0	70.0	45.0	92.1	0.4142
30.0	75.0	45.0	96.7	0.4045
30.0	80.0	45.0	101.4	0.3951
30.0	85.0	45.0	106.1	0.3862
30.0	0.0	60.0	30.0	0.5681
30.0	5.0	60.0	32.8	0.5613
30.0	10.0	60.0	36.0	0.5530
30.0	15.0	60.0	39.5	0.5437
30.0	20.0	60.0	43.3	0.5336
30.0	25.0	60.0	47.2	0.5229
30.0	30.0	60.0	51.3	0.5117
30.0	35.0	60.0	55.5	0.5002
30.0	40.0	60.0	59.8	0.4885
30.0	45.0	60.0	64.2	0.4768
30.0	50.0	60.0	68.6	0.4651
30.0	55.0	60.0	73.0	0.4535
30.0	60.0	60.0	77.5	0.4422
30.0	65.0	60.0	82.0	0.4310
30.0	70.0	60.0	86.5	0.4202
30.0	75.0	60.0	91.0	0.4098
30.0	80.0	60.0	95.5	0.3997
30.0	85.0	60.0	100.0	0.3901

APPENDIX IV-A (Continued)

Angle of Incidence	Angle of Observation	Azimuthal Angle,etc.	Magnitude of Phase Angle	Energy in Cal/cm^2 per min/ Steradian
30.0	0.0	75.0	30.0	0.5681
30.0	5.0	75.0	31.6	0.5640
30.0	10.0	75.0	33.9	0.5581
30.0	15.0	75.0	36.6	0.5507
30.0	20.0	75.0	39.7	0.5420
30.0	25.0	75.0	43.1	0.5324
30.0	30.0	75.0	46.7	0.5219
30.0	35.0	75.0	50.6	0.5108
30.0	40.0	75.0	54.5	0.4993
30.0	45.0	75.0	58.6	0.4875
30.0	50.0	75.0	62.8	0.4756
30.0	55.0	75.0	67.0	0.4635
30.0	60.0	75.0	71.3	0.4516
30.0	65.0	75.0	75.6	0.4397
30.0	70.0	75.0	79.9	0.4281
30.0	75.0	75.0	84.3	0.4167
30.0	80.0	75.0	88.7	0.4057
30.0	85.0	75.0	93.1	0.3950
30.0	0.0	90.0	30.0	0.5681
30.0	5.0	90.0	30.4	0.5671
30.0	10.0	90.0	31.5	0.5639
30.0	15.0	90.0	33.2	0.5588
30.0	20.0	90.0	35.5	0.5520
30.0	25.0	90.0	38.3	0.5438
30.0	30.0	90.0	41.4	0.5344
30.0	35.0	90.0	44.8	0.5239
30.0	40.0	90.0	48.4	0.5127
30.0	45.0	90.0	52.2	0.5009
30.0	50.0	90.0	56.2	0.4886
30.0	55.0	90.0	60.2	0.4761
30.0	60.0	90.0	64.3	0.4633
30.0	65.0	90.0	68.5	0.4506
30.0	70.0	90.0	72.8	0.4379
30.0	75.0	90.0	77.0	0.4253
30.0	80.0	90.0	81.4	0.4130
30.0	85.0	90.0	85.7	0.4010
30.0	0.0	105.0	30.0	0.5681
30.0	5.0	105.0	29.1	0.5702
30.0	10.0	105.0	28.9	0.5701
30.0	15.0	105.0	29.5	0.5678
30.0	20.0	105.0	30.9	0.5634
30.0	25.0	105.0	32.9	0.5570
30.0	30.0	105.0	35.4	0.5489
30.0	35.0	105.0	38.4	0.5394

APPENDIX IV-A (Continued)

Angle of Incidence	Angle of Observation	Azimuthal Angle,etc.	Magnitude of Phase Angle	Energy in Cal/cm^2 per min/ Steradian
30.0	40.0	105.0	41.7	0.5286
30.0	45.0	105.0	45.3	0.5169
30.0	50.0	105.0	49.0	0.5043
30.0	55.0	105.0	52.9	0.4911
30.0	60.0	105.0	57.0	0.4775
30.0	65.0	105.0	61.1	0.4636
30.0	70.0	105.0	65.3	0.4495
30.0	75.0	105.0	69.6	0.4355
30.0	80.0	105.0	73.9	0.4215
30.0	85.0	105.0	78.2	0.4078
30.0	0.0	120.0	30.0	0.5681
30.0	5.0	120.0	27.8	0.5733
30.0	10.0	120.0	26.3	0.5765
30.0	15.0	120.0	25.7	0.5773
30.0	20.0	120.0	25.9	0.5757
30.0	25.0	120.0	27.1	0.5716
30.0	30.0	120.0	29.0	0.5653
30.0	35.0	120.0	31.5	0.5569
30.0	40.0	120.0	34.5	0.5468
30.0	45.0	120.0	37.9	0.5352
30.0	50.0	120.0	41.6	0.5224
30.0	55.0	120.0	45.5	0.5086
30.0	60.0	120.0	49.5	0.4939
30.0	65.0	120.0	53.7	0.4787
30.0	70.0	120.0	57.9	0.4630
30.0	75.0	120.0	62.2	0.4470
30.0	80.0	120.0	66.6	0.4310
30.0	85.0	120.0	71.1	0.4151
30.0	0.0	135.0	30.0	0.5681
30.0	5.0	135.0	26.7	0.5761
30.0	10.0	135.0	23.9	0.5823
30.0	15.0	135.0	21.9	0.5865
30.0	20.0	135.0	20.8	0.5882
30.0	25.0	135.0	20.9	0.5869
30.0	30.0	135.0	22.1	0.5828
30.0	35.0	135.0	24.2	0.5759
30.0	40.0	135.0	27.0	0.5666
30.0	45.0	135.0	30.4	0.5553
30.0	50.0	135.0	34.2	0.5423
30.0	55.0	135.0	38.2	0.5277
30.0	60.0	135.0	42.3	0.5120
30.0	65.0	135.0	46.7	0.4952
30.0	70.0	135.0	51.1	0.4777
30.0	75.0	135.0	55.6	0.4595

APPENDIX IV-A (Continued)

Angle of Incidence	Angle of Observation	Azimuthal Angle,etc.	Magnitude of Phase Angle	Energy in Cal/cm^2 per min/ Steradian
30.0	80.0	135.0	60.1	0.4411
30.0	85.0	135.0	64.7	0.4225
30.0	0.0	150.0	30.0	0.5681
30.0	5.0	150.0	25.8	0.5782
30.0	10.0	150.0	21.9	0.5872
30.0	15.0	150.0	18.5	0.5947
30.0	20.0	150.0	15.9	0.5999
30.0	25.0	150.0	14.6	0.6020
30.0	30.0	150.0	14.9	0.6004
30.0	35.0	150.0	16.7	0.5950
30.0	40.0	150.0	19.7	0.5865
30.0	45.0	150.0	23.3	0.5753
30.0	50.0	150.0	27.3	0.5619
30.0	55.0	150.0	31.6	0.5467
30.0	60.0	150.0	36.1	0.5298
30.0	65.0	150.0	40.7	0.5116
30.0	70.0	150.0	45.3	0.4921
30.0	75.0	150.0	50.0	0.4717
30.0	80.0	150.0	54.8	0.4507
30.0	85.0	150.0	59.5	0.4292
30.0	0.0	165.0	30.0	0.5681
30.0	5.0	165.0	25.2	0.5796
30.0	10.0	165.0	20.5	0.5905
30.0	15.0	165.0	15.9	0.6005
30.0	20.0	165.0	11.8	0.6092
30.0	25.0	165.0	8.5	0.6153
30.0	30.0	165.0	7.5	0.6168
30.0	35.0	165.0	9.5	0.6124
30.0	40.0	165.0	13.1	0.6035
30.0	45.0	165.0	17.5	0.5918
30.0	50.0	165.0	22.1	0.5778
30.0	55.0	165.0	26.8	0.5617
30.0	60.0	165.0	31.6	0.5439
30.0	65.0	165.0	36.5	0.5244
30.0	70.0	165.0	41.4	0.5034
30.0	75.0	165.0	46.3	0.4812
30.0	80.0	165.0	51.2	0.4850
30.0	85.0	165.0	56.2	0.4342
30.0	0.0	180.0	30.0	0.5681
30.0	5.0	180.0	25.0	0.5801
30.0	10.0	180.0	20.0	0.5917
30.0	15.0	180.0	15.0	0.6027
30.0	20.0	180.0	10.0	0.6130

APPENDIX IV-A (Continued)

Angle of Incidence	Angle of Observation	Azimuthal Angle,etc.	Magnitude of Phase Angle	Energy in Cal/cm^2 per min/ Steradian
30.0	25.0	180.0	5.0	0.6223
30.0	30.0	180.0	0.0	0.6306
30.0	35.0	180.0	5.0	0.6220
30.0	40.0	180.0	10.0	0.6114
30.0	45.0	180.0	15.0	0.5988
30.0	50.0	180.0	20.0	0.5842
30.0	55.0	180.0	25.0	0.5677
30.0	60.0	180.0	30.0	0.5494
30.0	65.0	180.0	35.0	0.5294
30.0	70.0	180.0	40.0	0.5078
30.0	75.0	180.0	45.0	0.4849
30.0	80.0	180.0	50.0	0.4609
30.0	85.0	180.0	55.0	0.4361
0.0	0.0	0.0	0.0	0.6950
0.0	5.0	0.0	5.0	0.6878
0.0	10.0	0.0	10.0	0.6792
0.0	15.0	0.0	15.0	0.6693
0.0	20.0	0.0	20.0	0.6583
0.0	25.0	0.0	25.0	0.6462
0.0	30.0	0.0	30.0	0.6333
0.0	35.0	0.0	35.0	0.6197
0.0	40.0	0.0	40.0	0.6054
0.0	45.0	0.0	45.0	0.5905
0.0	50.0	0.0	50.0	0.5753
0.0	55.0	0.0	55.0	0.5598
0.0	60.0	0.0	60.0	0.5442
0.0	65.0	0.0	65.0	0.5285
0.0	70.0	0.0	70.0	0.5129
0.0	75.0	0.0	75.0	0.4974
0.0	80.0	0.0	80.0	0.4822
0.0	85.0	0.0	85.0	0.4674